A Short-Time Dynamics Study of Heisenberg Non-Collinear Magnets

by

Mirsaeed Zelli, B.Sc.

A Thesis
Submitted to the Faculty of Graduate Studies
in Partial Fulfillment of the Requirements
for the Degree of

MASTER OF SCIENCE

Department of Physics and Astronomy
University of Manitoba
Winnipeg, Manitoba

TABLE OF CONTENTS

LIST OF FIGURES

LIST OF TABLES

ACKNOWLEDGMENTS

I wish to express my deep and sincere gratitude to my advisor, Dr. Byron Southern for his continuous support, guidance and patience. I could not imagine having any better supervisor. I would like to thank my committee members, Dr. Randy Kobes of the University of Winnipeg and Dr. Mario Bieringer of the University of Manitoba. I would like to express my appreciation to the head of the department Dr. Peter Blunden. I also want to thank our secretaries Wanda Klassen and Susan Beshta for their help and assistance. I warmly thank Dr. Jason Fiege for his occasional hints. I wish to express my deepest appreciation to my family for their permanent support and endless love. In particular, I thank my father for the continuous inspiration that has been always pushing me forward. I would also like to acknowledge the financial support from the National Science and Engineering Research Council of Canada (NSERC) and the faculty of science. Finally, I acknowledge the high performance computational facilities at Westgrid.

ABSTRACT

A generalized model which describes a family of antiferromagnetic Heisenberg magnets on a three-dimensional stacked triangular lattice is introduced. The model contains a constraint parameter which changes the details of the interactions but not the symmetry of the model. We investigate the question of whether a first or second order phase transition occurs in these systems using a short time dynamics method. This method does not suffer from the problem of critical slowing down which occurs in the usual equilibrium Monte Carlo simulations. The effective critical exponents are determined as a function of the constraint parameter. Our results provide strong evidence that the phase transition is first order. In addition, for a particular value of the constraint parameter, the model corresponds to an antiferromagnet on a stacked Kagome lattice. In this case, our results are not inconsistent with the existence of a finite temperature first order phase transition.

Chapter 1

INTRODUCTION AND OVERVIEW

1.1 Introduction

Materials can be classified according to their magnetic properties as diamagnetic, paramagnetic, or ferromagnetic. Additional sublattice ordering such as antiferromagnets and ferrimagnets are also possible. In addition, often exotic magnetic phases such as spin glasses, spin ice and spin liquids can also occur in systems with disorder. The magnetic properties of materials originate microscopically from the magnetic moments of the particles within them. There are magnetic moments associated with both electrons and nuclei. The magnetic moment of the nucleus is much smaller than that of electrons and, in fact, it doesn't usually impact the magnetic properties of materials. The magnetic moment of an electron has two sources. One is due to the orbital motion of electrons around the nucleus. The other source is due to spin, an intrinsic characteristic of electrons that can only be understood from quantum mechanics. In this thesis, as we will be using the word "spin" frequently, it usually stands for the total magnetic moment of a particle from the experimental point of view.

In general, the magnetic properties are temperature dependent. A given compound which is paramagnetic at high temperature might make a transition from the paramagnetic phase to a ferromagnetic phase at a finite temperature called the Curie temperature. We say that the compound corresponds to a ferromagnetic system when the spins prefer to align in parallel. In the study of these magnetic materials, one often focuses on a temperature range around the Curie temperature called the critical

region. This is due to some peculiar and interesting characteristics associated with the phase transition. Some of these features are the creation of long-range magnetic structure by short-range interactions, the scaling behavior of different properties, and the existence of universality.

In order to make theoretical progress in understanding the physics of the phase transition, we usually introduce some spin models. The Hamiltonian associated with a model defines the detail and the range of interactions between spins. The spins are assumed to be classical. Quantum mechanical effects [2] are insignificant since, in the critical region, the thermodynamic behavior is determined by the domains of spins that are much larger than the length scales at which quantum effects are important. Due to the existence of planar or axial anisotropies in real materials, spins can be chosen as n-component spin vectors. Technically, $n = 1$ describes the materials with axial anisotropy. In the simplest case, the spins can take the values $+1$ or -1 value and the model is called the Ising model. For a planar spin system, the spins are confined to stay in a plane and the model is said to be the XY model ($n = 2$). In the case that spins are free to point in any direction on the surface of a sphere, the model is known as the Heisenberg model ($n = 3$).

A paramagnetic compound might make a transition to an antiferromagnetic phase as well. The transition temperature is known as the Néel temperature. We say that the compound corresponds to an antiferromagnetic system when spins favour an anti-parallel alignment. It is easy to see that the anti-parallel configuration can be reached in the square or cubic lattices with nearest neighbor interaction. However, it often happens that, either due to competing interactions or the specific geometry of the system, all the spins cannot establish an anti-parallel configuration. In other words, the energies of the bonds between spins cannot be minimized simultaneously. This phenomenon is called *frustration*. The type of frustration which is due entirely to the geometry is called geometrical frustration. The most familiar examples of this kind of frustration are stacked triangular antiferromagnets which are known as STA

models. The ground state of this model for XY and Heisenberg systems is a planar 120° structure. In contrast to non-frustrated systems, one cannot specify the ground state by only one vector. This leads to some changes in the nature of the phase transition associated with frustrated systems. It is the aim of this thesis to examine the critical behavior of the frustrated systems.

1.2 Overview of Thesis

During the past twenty five years, there has been a great deal of effort to clarify the nature of phase transitions associated with frustrated systems. In spite of the extensive amount of research work, the topic has remained a controversial subject. The peculiar critical behavior of a frustrated system can be due to the non-collinear structure of the ground state. This gives rise to a chiral degree of freedom which is believed to lead to either a new universality class of second order phase transitions or a weak first order phase transition [3].

The problem has been and still is the subject of experimental and numerical studies as well as theoretical analysis. Overall, the experimental studies have reported a second order phase transition. However the critical exponents were found to depend on the material under study. This questions the existence of universality and is inconsistent with a second order phase transition. In addition, the numerical studies have shown that universality is violated since the STA model and its modified version, the STAR model, exhibit different critical exponents. On the theoretical side, the situation is controversial because various field theoretical renormalization approaches have led to different results. The Landau-Ginzburg-Wilson model calculations favor a second order phase transition, in contrast to the non-perturbative methods which predict a weak first order phase transition.

The present work reports a numerical study of a family of Heisenberg STA magnets by means of Monte Carlo simulation. We introduce a generalized Hamiltonian

that contains the STA and STAR models as limits. Using a short time dynamics approach, we have determined the critical temperature and exponents of the model as a function of a constraint parameter r which does not change the symmetry of the model. The primary use of this model is to expose the non-universal behavior of Heisenberg frustrated magnets which is seen in experiments.

This thesis is organized in the following way. A general overview of some of the primary concepts of statistical mechanics and phase transitions are given in chapter 2. The phenomena of metastability and the role of breakdown of symmetry are briefly discussed. Chapter 3 is a brief review on the method of Monte Carlo simulation. Two of the most popular Monte Carlo algorithms and the method of finite size scaling are presented. In chapter 4, we introduce some of the frustrated models and also we summarize different studies on them from experimental, theoretical and numerical point of view. Chapter 5 is devoted to an introduction to the method of short-time dynamics in which the scaling relations of different quantities are derived. We present the results of the study on the generalized model in chapter 6. Finally, chapter 7 includes a summary of the results and an outlook of further research work on the problem.

Chapter 2

STATISTICAL MECHANICS AND PHASE TRANSITIONS

In this chapter we present some of the necessary background needed to understand the motivation and results of this thesis.

2.1 Review of Statistical Mechanics

Statistical mechanics is the method of dealing with systems consisting of many particles. It provides a framework to relate the macroscopic properties of systems to their microscopic characteristics. To establish these relations, various types of distributions are used. For example, for an isolated system in which the total energy is conserved, the most reasonable distribution is the microcanonical distribution. However, in this thesis, we consider systems that are in contact with heat reservoirs. A system in thermal equilibrium with a heat reservoir has a fixed temperature. The distribution that describes such a system is the canonical distribution. In the canonical distribution, the probability of finding the system in a microstate i which has energy E_i is

$$P_i = \frac{e^{-\beta E_i}}{Z} \tag{2.1}$$

where $\beta = 1/k_B T$, $k_B = 1.38 \times 10^{-23} JK^{-1}$ is Boltzmann's constant, and T is the temperature of the system. In equation (2.1), the denominator $Z = \sum_i e^{-\beta E_i}$ is a normalization factor called the partition function which is, in general, a function of temperature. Using this function, a useful thermodynamic potential is defined by

$$F = -k_B T \ln Z \tag{2.2}$$

where F is called *Helmholtz free energy*. The thermodynamic definition of Helmholtz free energy is

$$F = E - TS \tag{2.3}$$

where S is a crucial thermodynamic property called *entropy* and E is the internal energy of the system. All the thermodynamic quantities can be calculated from this potential and its derivatives. From equation (2.1), we can calculate the thermal average value of any property X of the system by

$$\langle X \rangle = \frac{1}{Z} \sum_i X_i e^{-\beta E_i} \tag{2.4}$$

where X_i is the value of the property for the microstate i. For example, the average value of energy is

$$\langle E \rangle = \frac{1}{Z} \sum_i E_i e^{-\beta E_i} = \partial(\beta F)/\partial\beta \tag{2.5}$$

where the last part of the equation emphasizes that E, a macroscopic property, can be derived from Helmholtz free energy. There are other properties that are also of interest. Response functions are defined as the response of the system to small changes of parameters such as temperature which are controlled externally. One of the important response functions is specific heat, defined by

$$C_v = \frac{\partial E}{\partial T} = -k_B \beta^2 \frac{\partial E}{\partial \beta}. \tag{2.6}$$

It can also be shown that specific heat is closely related to fluctuations of energy around its mean value. Another important response function is susceptibility. Because we are working with magnetic systems, it is appropriate to have a thermodynamic definition of magnetic susceptibility as follows

$$\chi = \frac{\partial M}{\partial h} \mid_T = \frac{-1}{\beta} \frac{\partial^2}{\partial h^2} (\beta F) \mid_T \tag{2.7}$$

where M is the total magnetization and h is the magnetic field. Magnetic susceptibility is closely related to magnetization fluctuations. In general, the fluctuations in

energy and magnetization increase as the system becomes larger but the fractional fluctuations, defined by $\delta X/X$ where δX is the RMS (root mean square) of the fluctuation in X, tend to fall as the inverse square root of the system size. As a result, they vanish in the limit of infinite size system which is called *thermodynamic limit* [4].

2.2 Phase transitions

Phase is a region in which the thermodynamic properties of the system under consideration remain analytic. In other words, different phases are represented by different free energy functions. When a system undergoes a phase transition, it changes from one phase to another in which some of the physical characteristics are different. Phase transitions are crucial to the life on earth, and so their study constitutes a broad branch of condensed matter physics.

2.2.1 Order parameter

In order to make some theoretical progress on the description of phase transitions, we have to identify a parameter called an *order parameter*. The value of the order parameter vanishes on one side of the transition but has a nonzero value on other side of the transition. We define different order parameters for different systems. In a liquid-gas system the order parameter is the difference between the liquid and gas densities, but in a ferromagnet it is simply the magnetization per volume or the magnetization per spin defined by $m = M/N$, where N is the total number of spins in the system [4]. For an antiferromagnetic system on a square lattice the order parameter is the magnetization per spin of one of the sublattices. Because there is no general scheme for defining order parameters, an appropriate definition of the order parameter for a particular system is crucial.

2.2.2 First order and second order phase transitions

Phase transitions are classified as *first order* or *second order*. If the first derivatives of free energy with respect to the intensive parameters such as temperature are discontinuous, the transition is a first order transition. It simply means that, for a first order transition, the free energy curves of the ordered and disordered phases cross each other with a finite difference in slope. All first order transitions involve a *latent heat*. The paradigm of a first order phase transition is the ordinary freezing of water at its freezing point.

By contrast, if the first derivative of free energy is continuous, the transition is categorized as *a continuous phase transition* or *a second order phase transition*. In other words, the free energy curves of the two phases meet tangentially at a second order phase transition. There is no latent heat involved and the order parameter increases continuously from zero. What changes discontinuously at the phase transition is the rate of change in the order parameter. More generally, the second derivatives of the free energy are singular when the phase transition occurs. This is the reason we call it a second order phase transition. The temperature at which a second order phase transition occurs is called the critical temperature T_c. A simple example of this type of phase transition is that of iron from the paramagnetic to the ferromagnetic phase. The transition temperature for a second order phase transition is called critical temperature T_c.

2.2.3 Correlation functions and critical exponents

For a spin system, we are interested in how correlated the spins are at different sites, or in other words, how large are the regions where the spins have almost the same direction even if the system is disordered. To make some progress, the first step is the introduction of a *correlation function*

$$G(r) = \langle \rho(0)\rho(r) \rangle \tag{2.8}$$

where r is the spatial distance and ρ is the order parameter of the system under consideration. For a discrete spin system, ρ stands for the spin at different sites. The expression (2.8) is useful only when the expectation value of ρ is zero. In order to make it more general, we define the *connected correlation function* as follows

$$G_c(r) = \langle \rho(0)\rho(r) \rangle - \langle \rho(0) \rangle \langle \rho(r) \rangle \tag{2.9}$$

where we have excluded the contribution to $\langle \rho(0)\rho(r) \rangle$ that comes from the $\langle \rho \rangle$ itself. For a system that undergoes a second order phase transition, there is an asymptotic relation of $G_c(r)$ for large r at $T = T_c$ [4] as follows

$$G_c(r) \sim \frac{1}{r^{d-2+\eta}} \tag{2.10}$$

where d is the spatial dimensionality of the system and and η is a critical exponent called *the anomalous dimension*. In general it is appropriate to define the reduced temperature τ as

$$\tau = \frac{T - T_c}{T_c}. \tag{2.11}$$

For small τ which implies a temperature close to T_c, one can approximate (2.10) by

$$G_c(r) \sim \frac{1}{r^{d-2+\eta}} e^{-r/\xi} \tag{2.12}$$

where ξ is a parameter with the dimension of length and is called the *correlation length*. Equation (2.12) is, in fact, the definition of the correlation length. ξ is the parameter that measures the size of regions where spins are correlated. The important characteristic of ξ is its divergence at T_c in the thermodynamic limit with a power law behaviour

$$\xi \sim |\tau|^{-\nu} \tag{2.13}$$

where ν is another critical exponent. Correlation length is not the only quantity that shows power law behaviour as we define other critical exponents in the vicinity of T_c as follows:

Specific heat	$C_v \sim \lvert\tau\rvert^{-\alpha}$	$\tau > 0$
	$C_v \sim \lvert\tau\rvert^{-\alpha'}$	$\tau < 0$
Susceptibility	$\chi \sim \lvert\tau\rvert^{-\gamma}$	$\tau > 0$
	$\chi \sim \lvert\tau\rvert^{-\gamma'}$	$\tau < 0$
Order parameter	$m \sim \lvert\tau\rvert^{\beta}$	$\tau < 0$

(2.14)

In general the critical exponents on both sides of the critical point are the same but the prefactors of the power laws will be different.

2.2.4 Scaling laws and universality

All the critical exponents are not independent as they are related to each other through some relations called *scaling laws*. Some of the scaling laws are the following:

$$\alpha + 2\beta + \gamma = 2 \tag{2.15}$$

$$d\nu = \gamma + 2\beta \tag{2.16}$$

$$\gamma = \nu(2 - \eta) \tag{2.17}$$

$$\beta = \frac{1}{2}(d - 2 + \eta)\nu. \tag{2.18}$$

In fact only two of the critical exponents are independent. Experiments conducted to measure the critical exponents conclude that some systems with very different transitions exhibit the same critical behavior. This phenomenon is called *universality* and all the systems with sets of the same critical exponents form a universality class. It turns out that the universality class of one system depends on the dimensionality d of the system and the dimensionality n of the order parameter. There are a few other factors that might be important in determination of the universality class of one system such as the presence of symmetry breaking field, but the remarkable thing

is that the details of the interactions between particles are irrelevant. For example, ferromagnetic Ising systems on the square and the triangular lattices belong to the same universality class.

2.3 Metastability

We know that a system at a given temperature is stable if its free energy is in a minimum. If the minimum is just a local one, then the state of the system is a metastable state. Even though there exists a global minimum for the free energy which represents the most stable state, the system simply may not have enough thermal fluctuations to overcome the energy barrier between the local and global minima. As a matter of fact, some systems spend a long time in a metastable state before they find their lowest energy states. It often happens that we measure different properties of systems while they are metastable during the time interval that the experiment is conducted. A good example of this situation is the measurement of the hysteresis loop of ferromagnets. Even though the magnetization is in opposite direction of the magnetic field, which is energetically unfavorable, it remains almost constant as the measurements are performed. In cases like this, if we are to obtain, by statistical calculations, some results in agreement with experiments, we have to artificially restrict the sum over microstates to those states which are accessible to the system during the course of the experiment.

Metastability, as latent heat, is a common property of first order phase transitions. When a system makes a first order transition from a high-temperature phase to a low-temperature phase under certain circumstances the practical phase transition doesn't occur exactly at the real transition temperature T_t. In other words, as the system cools through the T_t, it persists below the phase transition. Therefore, in a small temperature range below the T_t, the system is in a local minimum state (high-temperature phase) which doesn't jump to a global minimum state (low-temperature

phase) with just a small perturbation.

2.4 Spontaneous Breakdown of Symmetry

Once a ferromagnetic system undergoes a phase transition at the Curie temperature, then there is a spontaneous magnetization. The direction of the magnetization defines an unique direction in space, whereas above the Curie temperature there is no special direction and the space is homogeneous. The appearance of the unique direction reduces the symmetry of the system to a lower symmetry. This is called breakdown of symmetry (BS). In general, every system possesses a symmetry group whose symmetry operators leave the Hamiltonian associated with the system invariant. As the phase transition takes place, the ordered state does not reflect the full symmetry of the Hamiltonian, so we say that there exists a spontaneous breakdown of symmetry accompanied with the phase transition.

The actual process by which the direction of the broken symmetry is chosen is irrelevant but one should be careful when calculating the magnetization. If the partition function is calculated by summing over all the states of the system, magnetization will vanish. So it seems that there is a discrepancy between statistical mechanics and experiments. In fact the situation is a bit similar to the one for metastable systems. By summing over all the possible states, we neglect the fact that most of them don't contribute to the partition function which is experimentally measured in a limited period of time. In other words, spontaneous symmetry breaking is always accompanied by ergodicity breaking. This tells us that the system is effectively trapped in a region of configurations. In order to acquire a realistic magnetization, we must therefore restrict the number of microscopic states over which the summation in the partition function is performed.

The BS can be described by the symmetry groups before and after the transition. These symmetry groups are either continuous or discrete. Discrete symmetry groups

have a finite number of elements, in contrast to continuous symmetry groups which possess an uncountable continuum of elements. To understand the situation, it is appropriate to study the n-vector model.

2.4.1 n-vector model

The n-vector model is described by the following Hamiltonian

$$H = -J \sum_{<ij>} \vec{S}_i \cdot \vec{S}_j \tag{2.19}$$

where $\vec{S}_i$ are n component classical spin vectors, J is the interaction constant and $< ij >$ denotes the fact that only nearest neighbors interact. For ferromagnetic systems the interaction constant J is positive, but it is negative for antiferromagnetic systems. Since the Hamiltonian is rotationally invariant, the symmetry group is the $O(n)$ symmetry group which is the orthogonal transformation group of n-dimensional Euclidean space. This symmetry group corresponds to the highest symmetry that a system with n-component order parameter can possibly have. $O(n)$ symmetry group consists of the proper and improper rotational symmetry groups. Therefore, one may write

$$O(n) = Z_2 \times SO(n) \tag{2.20}$$

where $SO(n)$ is the proper rotational symmetry group and Z_2 is the reflection operator that takes care of the improper part of the $O(n)$ symmetry group. Since $O(1) = Z_2$, we have $SO(1) = 1$. By definition, we also have $O(0) = 1$, the identity group.

For $n = 1$, the model is an Ising spin model possessing the discrete $O(1) = Z_2$ symmetry group. This symmetry group, called sometimes the time-reversal symmetry group, is due to invariance of the Hamiltonian under reversing the direction of all spins. For any $n \geqslant 2$, the symmetry group becomes continuous. In the $n = 2$ case, the Hamiltonian corresponds to the XY spin model which possess $O(2)$ symmetry. For $n = 3$, the n-vector model is the so-called Heisenberg spin model which has the $O(3)$ symmetry group.

2.4.2 Order Parameter Space

Order parameter space is a topological space formed by all possible values of the order parameter. In the case of the ferromagnetic Heisenberg model, for instance, this space is isomorphic to the two-dimensional surface of a unit sphere. Order parameter space can be defined by dividing the full symmetry group of the Hamiltonian by the reduced (broken) symmetry group of the ordered state [5]. The broken symmetry group of the ordered state is always the subgroup of the full symmetry group that leaves the order parameter unchanged. In the case of the ferromagnetic Heisenberg model, $O(2)$ is the subgroup of rotations about the magnetization axis. Hence, the order parameter space is $O(3)/O(2)$ which is equivalent to $SO(3)/SO(2)$. In general, for ferromagnetic spin models with n components, the broken symmetry group is $O(n-1)$, the subgroup of $O(n)$ which corresponds to rotations about the direction of the broken symmetry. This leads to the order parameter space $O(n)/O(n-1)$.

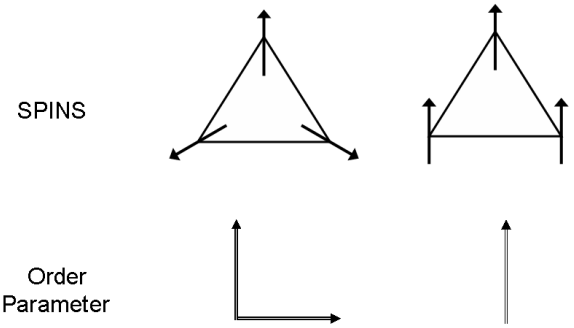

Figure 2.1: The order parameters for collinear and non-collinear systems

In the above discussion, the ferromagnetic requirement is not an essential one. In fact, $O(n)/O(n-1)$ is the order parameter space for non-frustrated spin models which have a collinear ground state (GS). We say collinear in a sense that only one vector is enough to specify the direction of the broken symmetry. By contrast, one needs at least two vectors to specify the directions of the broken symmetry in a non-collinear GS. Figure 2.1 shows the situation in which two order parameter vectors are

needed to specify the BS of a frustrated system with a non-collinear 120° structure at low temperature. As a result, the broken symmetry group for such a system will be $O(n-2)$.This introduces the order parameter space $O(n)/O(n-2)$. In the $n=2$ case, the order parameter space is $O(2)$ which differs from $SO(2)$ of the non-frustrated collinear systems. In the $n=3$ case, it is $SO(3)$ since

$$O(3)/O(1) = Z_2 \times SO(3)/Z_2 = SO(3). \tag{2.21}$$

BS plays a crucial role in establishing the universality classes of systems. BS itself is described by the order parameter space. In fact, they are the same concept. For example, we may say that the BS of non-frustrated spin models is $O(n)/O(n-1)$. As a result, all the systems possessing the $O(n)/O(n-1)$ BS exhibit the same critical behavior and belong to the same universality class, the so-called Wilson-Fisher universality class [6]. However, the situation is more complicated for frustrated non-collinear systems. In particular, we are interested in systems with the BS $O(n)/O(n-2)$. The paradigm of such systems is STA model with a non-collinear 120° structure of the GS. The nature of the phase transitions associated with these systems has remained unclear and is still a controversial subject to investigate.

Chapter 3

MONTE CARLO SIMULATION

3.1 Introduction

There exist only a few statistical models that have an exact analytical solution, so that one must use approximation methods in order to deal with the majority of statistical models. With the continuous improvements in the technology of CPU's and memory, numerical approximation methods have been exploited to achieve reliable solutions to these statistical problems. The most well-known numerical approximation method is the Monte Carlo (MC) method which is widely used in all areas of science. The Monte Carlo method is one of the most powerful methods of computation in physics. Its name emphasizes its stochastic characteristic which is the main difference between the MC method and other numerical methods such as molecular dynamics.

This chapter is devoted to an introduction of the MC method. We first explain how MC works, and then we introduce the two common algorithms of MC calculations. This will be followed by a brief discussion about the ways of applying MC simulation as well as error estimation of MC measurements. Finally, we will consider the method of finite size scaling which is a popular method of extrapolating the MC data to the thermodynamic limit.

3.2 How does MC work?

Generally, physical systems consist of a vast number of particles, such that the number of summations in the partition function is numerically unreachable. So, doing numerical calculations, we are only able to sample a small portion of the partition

function. Basically MC provides us with the techniques to select the most probable states in our sample. In a Monte Carlo simulation the idea is to generate states by a stochastic process such that the probability of a state is given by the appropriate distribution.

The most common distribution is the canonical distribution where we wish to find the thermal average of a quantity of interest, X. Of course, the exact value can be obtained if we go through all the available states in our system. However the number of our observations is limited, and the best we can do is to increase the number of observations q, so that the estimator of X is given by

$$X_q = \frac{\sum_{i=1}^{q} X_i e^{-\beta E_i}}{\sum_{i=1}^{q} e^{-\beta E_i}} \tag{3.1}$$

where X_i is the value of X for state i of our sample. It turns out that this estimator is a rather poor one because the majority of states over which the summation is performed do not contribute significantly to X_q. This is quite clear at low temperature, where the system spends most of its time in the ground state and the value of $e^{-\beta E_i}$ is very small for any excited state. Hence another estimator is introduced as follows

$$X_q = \frac{\sum_{i=1}^{q} X_i p_i^{-1} e^{-\beta E_i}}{\sum_{i=1}^{q} p_i^{-1} e^{-\beta E_i}} \tag{3.2}$$

where p_i is the probability of choosing state i as one of the states in our sample. If one singles out all the states of the sample at random, which means $p_i = constant$, then the equation will reduce to equation (3.1). The best choice of p_i is $p_i = e^{-\beta E_i} / \sum_i e^{-\beta E_i}$ such that the formula for the estimator (3.2) becomes simply:

$$X_q = \frac{1}{q} \sum_{i=1}^{q} X_i. \tag{3.3}$$

This is called importance sampling which means that we sample the important states that make larger contributions to the quantities we are trying to estimate. By using importance sampling, the variance of the estimator decreases considerably which indicates that a more precise result is achieved. To understand how we select states

according to the Boltzmann distribution by a stochastic process, one should consider the general theory of Markov processes.

3.2.1 Markov processes

To sample our states according to the Boltzmann distribution, it is not efficient to choose one state and then accept or reject it with a probability $e^{-\beta E_i}$. Instead, Markov processes present us a very efficient way to do so. Markov process is a rule to generate a new configuration of a system from the present one in a random fashion. The generation of the new configuration does not rely on the history of the system and only depends on the current configuration. For each possible pair of states μ and ν there exists a probability $P(\mu \to \nu)$ which is the probability of transition from state μ to state ν. The transition probabilities should be non-negative and time independent. They must also satisfy the following constraint

$$\sum_{\nu} P(\mu \to \nu) = 1 \tag{3.4}$$

which implies that there is always a transition at each step. Successive use of the Markov process results in a sequence of states called a Markov chain. Technically, as the Markov chain gets longer, the number of occurrences of each state μ converges to the Boltzmann weighting factor $e^{-\beta E_\mu}$ times a constant value which depends only on the length of the chain.

To ensure that thermal equilibrium is accomplished after waiting for a suitable period of time, we must impose two other conditions: ergodicity and detailed balance.

Ergodicity

Ergodicity signifies that from each state ν, there should be a non-zero probability to reach another state μ in a sufficient but finite length of time. This requirement ensures that the system will not be trapped in a limited number of configurations

so that every state will eventually be visited. It should be noted that the condition might be satisfied even if several direct transition probabilities $P(\mu \to \nu)$ are zero.

Detailed balance

The condition of detailed balance is described as follows:

$$p_\nu P(\nu \to \mu) = p_\mu P(\mu \to \nu). \tag{3.5}$$

This condition is derived as a result of the requirement which ensures that the rate of gain and loss of each state is equal once the equilibrium is established. We can rewrite the detailed balance equation for the Boltzmann distribution as follows:

$$\frac{P(\mu \to \nu)}{P(\nu \to \mu)} = \frac{p_\nu}{p_\mu} = e^{-\beta(E_\nu - E_\mu)}. \tag{3.6}$$

One notices that we have the freedom to select $P(\mu \to \nu)$ as long as the ratio $P(\mu \to \nu)/P(\nu \to \mu)$ satisfies equation (3.6). This freedom leads to different kinds of MC algorithms. In general, MC algorithms are categorized into two: single-spin flipping algorithms such as Metropolis algorithm and cluster flip algorithms [7, 8] like the Wolff algorithm. All the calculations done in this thesis have used single-spin flip algorithms, so a bit background about them seems to be necessary.

3.3 The single-spin flip algorithms

A single-spin flip algorithm, as its name implies, updates only one spin in each step. The most common single-spin flip algorithms are the Metropolis algorithm and the heat-bath algorithm:

3.3.1 The Metropolis algorithm

The Metropolis algorithm [9] is the most famous MC algorithm which has been applied to a vast variety of problems. In the Metropolis algorithm, equation (3.6) is satisfied

by the following choice of transition probability:

$$P(\mu \to \nu) \quad = A^{-1} e^{-\beta(E_\nu - E_\mu)} \qquad E_\nu > E_\mu \tag{3.7}$$

$$= A^{-1} \qquad E_\nu < E_\mu$$

where A is a normalization constant. Briefly, it relies on acceptance or rejection of random movements from the current configurations. The general procedure of implementing the Metropolis algorithm is as follows:

1. Choose an initial configuration which is usually chosen to be a random state;

2. Choose a lattice site i which can be selected either at random or in order. The preference might differ from case to case;

3. Make a move by choosing a new random direction. Of course in the case of Ising model, there are only two directions;

4. Calculate the energy difference $\Delta E = E_{new} - E_{old}$;

5. If $\Delta E < 0$, then accept the move;

6. If $\Delta E > 0$, then generate a random number r in the range [0,1];

7. If $r \leqslant e^{-\beta \Delta E}$, then accept the move;

8. go back to the step number 2 and repeat the process;

The reader sees that the nature of moves is entirely arbitrary. This makes the algorithm very general and also practically straightforward to implement. In fact this is one of the main reasons it is such a popular algorithm.

3.3.2 The heat-bath algorithm

In several cases the Metropolis algorithm is not as efficient as we desire, so one should think about alternative algorithms. One of these alternative methods is the heat-bath algorithm which has been proven to be quite effective for many problems. A notable feature of the algorithm is that there is always a spin update. In other words there is always a change in the direction of the spin that is being updated, even though the change might be small at low temperature. Hence, heat-bath provides an efficient way to select the accessible microstates. The heat-bath algorithm can be applied to discrete or continuous spin systems. The systems that we are interested in are the three component continuous spin systems ($n = 3$) which can in general be described by the following Hamiltonian:

$$H = -J \sum_{<ij>} \vec{S}_i \cdot \vec{S}_j - (\sum_i \vec{S}_i) \cdot \vec{B}_{ext} \tag{3.8}$$

where $\vec{B}_{ext}$ is the external field and $< ij >$ signifies that the sum is over the nearest neighbors. We can generalize the Hamiltonian by inserting some anisotropies. Nevertheless, it doesn't change the generality of the discussion. The way the heat-bath algorithm works relies on the definition of some local fields for each lattice site i using

$$\vec{B}_i = -\partial H / \partial \vec{S}_i = \vec{B}_{nei} + \vec{B}_{ext} \tag{3.9}$$

where $\vec{B}_{nei}$ is the local field vector imposed by all the nearest neighboring spins of the spin at site i. The part of the Hamiltonian which is due to $\vec{S}_i$ is simply

$$h_i = -\vec{S}_i \cdot \vec{B}_i = -|B_i| \cos(\theta) \tag{3.10}$$

where θ is the angle between the spin and the local field. Assuming that the direction of $\vec{B}_i$ is in the z direction (note that this z direction is a local z direction and differs from the real z direction we select from the start), the probability of finding the spin in a small element of solid angle $d\omega = \sin(\theta) d\phi d\theta$ (remember that we need only two

angles to specify the direction of each spin) is

$$P(\theta, \phi) = C \exp(-\beta h_i) = C \exp(\beta |B_i| \cos(\theta)) \tag{3.11}$$

where C is a normalization factor. The probability function does not depend on the angle ϕ, so ϕ can be chosen from a uniform random distribution in the interval $[0, 2\pi]$. Now all we need is a random number generator which gives us the right distribution of $\cos(\theta)$ based on the value of $b_{ieff} = \beta |B_i|$. This can be accomplished by using the following formula (see Appendix A)

$$\cos(\theta) = 1 + \ln[(1 - r1) exp(-2b_{ieff}) + r1]/b_{ieff}. \tag{3.12}$$

where $r1$ is a random number in the range $[0, 1]$ generated by an uniform random number generator. At the final step , using Euler angles, we should rotate the spin so that the local coordinate system, which has its z direction parallel to the direction of the local magnetic field, to be the same as the global coordinate system.

3.4 How do we apply MC?

To start MC calculations, we first specify the geometry and all the interactions in the system. Afterwards, because all the systems we study are finite size systems, it is required to impose boundary conditions. The most common boundary condition is a *periodic boundary condition* which makes all the spins on one edge of the lattice see the spins on other edge as their neighbors. Once the periodic boundary condition is imposed, then one might think of the system as a infinite sized system which is invariant under translation by L where L is the linear size of the cluster being updated.

3.4.1 Equilibrium vs out-of-equilibrium simulation

The two conditions of ergodicity and detailed balance ensure that equilibrium is established after a reasonable length of time. The primary intention of using MC is to

calculate the quantities of interest in equilibrium. To do so, we initialize the system in a state of complete disorder which represents a high temperature considerably above the T_c, and then we gradually cool down the system. Every time the temperature is reduced by a small amount ΔT, we should discard a sufficient number of MC steps, called the equilibration time τ_{eq}, which is the amount of time our system needs to reach the new equilibrium. Afterwards, we start to measure the quantities of interest, such as energy, specific heat, and the order parameter, using equation (3.3). Of course, the number of measurements must also be sufficiently large in order to obtain a relatively small variance of the quantity around its average value.

Although various MC algorithms have different characteristics, they all return the same result as long as a sufficiently large number of measurements are performed in equilibrium. However, the situation is more complicated if we intend to simulate the relaxation process of a system toward equilibrium. A system in the relaxation process, which is far away from equilibrium, chooses a path toward equilibrium according to the MC algorithm we have applied. Technically, we say different algorithms introduce different dynamics. This area of MC simulation is a less well-developed area compared to the one for equilibrium simulation, and one should be careful to choose the right dynamics. In particular we are interested in the critical relaxation process. This interest is due to the presence of a general scaling form that enables us to calculate T_c and the critical exponents of different systems far from equilibrium [10, 11]. This process will be discussed further in the following chapters.

3.5 Statistical error of Monte Carlo measurements

There is always some statistical error associated with calculations that involve random numbers. Let us assume that we have q independent measurements X_i that are distributed according to a Gaussian distribution. If the width of the Gaussian distribution is σ, then it can be shown that the standard error of the estimator (3.1)

is [12]

$$error = \sigma/\sqrt{q}\ . \tag{3.13}$$

The σ itself can be approximated from the data [12] as follows

$$\sigma^2 \simeq \frac{q}{q-1}(\overline{X^2} - (\overline{X})^2) = \frac{1}{q-1}\sum_{i=1}^{q}(X_i - \overline{X})^2. \tag{3.14}$$

Hence the error is

$$error = \Delta X = \sqrt{(\overline{X^2} - (\overline{X})^2)/(q-1)}. \tag{3.15}$$

One sees that the magnitude of error falls as $q^{-1/2}$. A reasonable number of measurements is one that gives us a sufficiently small ratio $\Delta X/X$. It should be noted that equation (3.15) is valid only when all of the observations are independent. Otherwise, for correlated observations, we should replace it [13] by

$$error = \sqrt{\frac{\overline{X^2} - (\overline{X})^2}{q-1}(1 + 2\tau_c/\delta t)} \tag{3.16}$$

where δt is the time interval between subsequent observations and τ_c called correlation time is about to be described in the next section.

3.6 Correlation time and critical slowing down

It is useful to define a quantity that tells us how correlated the configurations of a system are at different times. This quantity, called the correlation time, is a measure of how many updates have to be made before we have two independent states. First we define a relaxation function in equilibrium as follows

$$\phi(t) = \int_{t_i}^{t_f - t} dt'[m(t')m(t'+t) - \langle m\rangle^2] \tag{3.17}$$

where t_i can be any time after reaching the equilibrium and t_f is the time we stopped measuring. Also $m(t)$ is the magnetization of the system at time t and $\langle m\rangle$ is the average value. The relaxation function behaves exponentially at long times as follows

$$\phi(t) \sim e^{-t/\tau_c} \tag{3.18}$$

where τ_c is the correlation time. The correlation time can be expressed in terms of correlation length ξ

$$\tau_c \propto \xi^z \propto |\tau|^{-\nu z} \tag{3.19}$$

where z is a new, positive exponent. This exponent differs from the previous exponents we introduced, since it is a dynamic one. Its value depends on the algorithm which performs the updating and not merely on the model.

According to equation (3.19), the correlation time τ_c diverges as T_c is approached ($\tau = 0$). This means that, near the critical region, the successive measurements that we perform are not independent for a long time. This phenomenon, which is called *critical slowing down*, causes considerable reduction in the accuracy of MC results, and therefore long simulation times are required.

3.7 Finite size scaling method

In chapter 2, it was pointed out that, in the thermodynamic limit, susceptibility and specific heat diverge at the critical point T_c and they exhibit power law behavior with appropriate critical exponents. However, there is no divergence for a finite size system. Instead, there exists a whole critical region where these quantities possess their maximum values for different sizes. Generally speaking, the positions of the maxima shift as a function of L such that it finally approaches the exact T_c as $L \to \infty$. This is due to the fact that the correlation length of a finite size system cannot become larger than the size L of the system. This results in a cut-off value for divergent properties. Even for the order parameter, which does not diverge, the finite size effect is apparent as shown in fig. 3.1 for the two-dimensional Ising model. One can see the convergence of the order parameter to the thermodynamic limit behavior as L increases. It is worth to note that, for systems of this type, we should measure the absolute value of the magnetization $|m|$ rather than m. This is because, even in an ordered region, the order parameter changes sign for a sufficiently long run due to

the finite size effects. As a result, the mean value of the magnetization is zero at any temperature as long as we perform enough updating.

Hence one may think that MC simulation, which can only be applied to finite size systems, would be rather ineffective to obtain accurate critical exponents. However, there is a method called *finite size scaling method* (FSS) that provides the techniques to extrapolate the result to the thermodynamic limit. It also enables us to distinguish the order of the phase transition. The basic idea of FSS is the introduction of a scaling

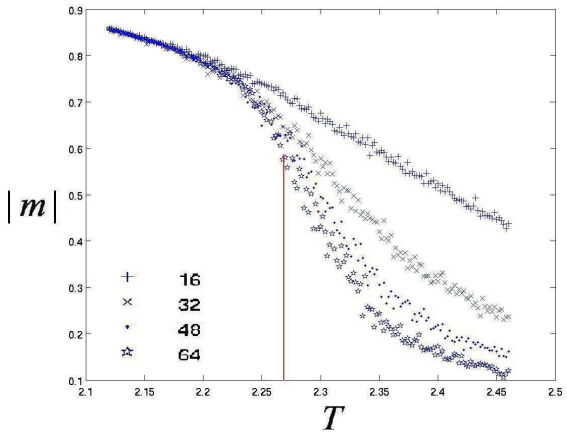

Figure 3.1: The magnetization of two-dimensional Ising model for different linear system sizes. The solid line corresponds to the exact solution of Onsager [1] with $T_c = 2.269$. One notices that the $|m|$ is always non-zero for finite size systems.

form of free energy [6, 14, 13] as follows

$$F(\tau, L) = L^{(\alpha-2)/\nu} F'(\tau L^{1/\nu}) \tag{3.20}$$

where τ is the reduced temperature and $\tau L^{1/\nu}$ is a scaling variable. This scaling form is only valid for sufficiently large systems in the critical region. By appropriate differentiation of the free energy, the scaling forms of various properties are derived as follows

$$m = L^{-\beta/\nu} m'(\tau L^{1/\nu}) \tag{3.21}$$

$$\chi = L^{\gamma/\nu}\chi'(\tau L^{1/\nu}) \tag{3.22}$$

$$C = L^{\alpha/\nu}C'(\tau L^{1/\nu}) \tag{3.23}$$

where C', χ', and M' are the scaling functions. At $\tau = 0$ ($T = T_c$), the scaling forms reduce to

$$m \propto L^{-\beta/\nu} \tag{3.24}$$

$$\chi \propto L^{\gamma/\nu} \tag{3.25}$$

$$C \propto L^{\alpha/\nu}. \tag{3.26}$$

which can be exploited directly to estimate the critical exponents, provided that ν is already known. However, a more powerful tool is to collapse the data where we plot the scaling functions with respect to their argument, the scaling variable. Since the scaling function is the same for all system sizes, all the curves for different sizes L must be mapped into a unique curve. For instance, the analysis of the raw data of fig. 3.1 shows that, for the exponent value $\beta = 1/8$ and $\nu = 1$, the data of different sizes collapse to a single curve. The situation is shown in fig. 3.2(a) where $m'(\tau L^{1/\nu}) = mL^{\beta/\nu}$ is plotted as a function of $\tau L^{1/\nu}$. In addition, in fig. 3.2(b), we have shown the scaling function versus the scaling variable on a log-log scale. The scaling analysis tells us that for $T < T_c$, the slope of the linear behavior is β. However, for $T > T_c$, the slope will be $\beta - \nu d/2$.

It is worth mentioning that the scaling form of the correlation length is

$$\xi = L\,\xi'(\tau L^{1/\nu}) \tag{3.27}$$

which enables us to calculate the critical exponent ν directly. In addition, there is a useful quantity, the reduced fourth order cumulant of the order parameter [15], defined by

$$U_4 = 1 - \frac{\langle m^4 \rangle}{3\langle m^2 \rangle^2}. \tag{3.28}$$

The U_4 curves for sufficiently large sizes cross each other at the critical temperature T_c. This allows us to find T_c with good precision.

We point out that for a strong first order transition, the correlation length doesn't diverge, so the scaling form of a second phase transition can not be used. Instead, the specific heat and susceptibility scale as the volume of the system L^d. In fact, this kind of scaling behavior is often used as an indication of the existence of a first order phase transition [16, 17].

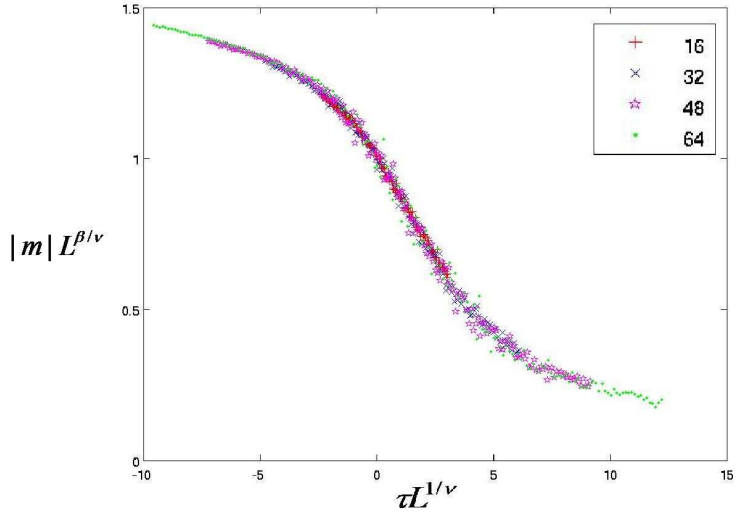

(a)

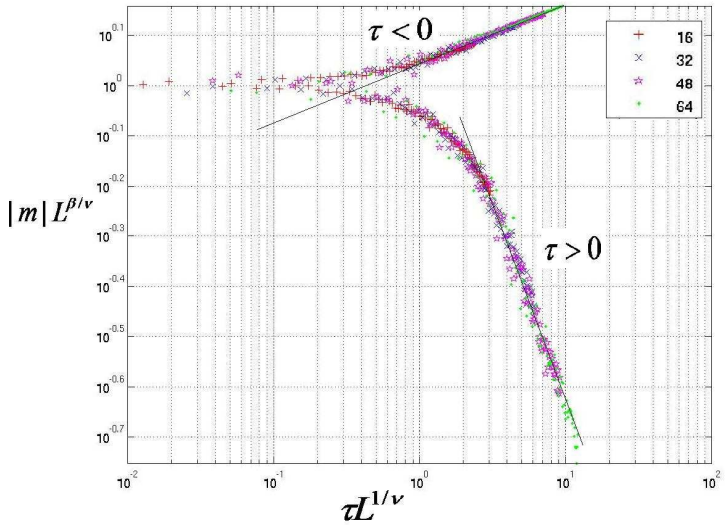

(b)

Figure 3.2: The scaling function of magnetization in $2d$ Ising model as a function of the scaling variable (a) on a normal scale and (b) on a log-log scale

Chapter 4

FRUSTRATION

4.1 Introduction

A system is *frustrated* when the global ordering of the system is not compatible with the local ordering of its particles. For a spin system, this means that the energy of all the interactions between spins cannot be minimized simultaneously. The effect of frustration is important and unexpected, so that great efforts of research have been made to gain more insight into the phenomenon of frustration. In particular, much attention has been focused on the nature of the phase transitions associated with frustrated systems. An important question which has to be answered is whether the phase transition is second order or first order. Subsequently, we must ask to which universality class it belongs if it is a second order phase transition. It is the aim of this chapter to consider the different approaches which have been used to answer these two questions. We first introduce some of the important frustrated models and then we briefly discuss the experimental studies of frustrated magnets. Afterwards we describe the different theoretical approaches to the problem to clarify the current situation of our understanding of the critical behavior of frustrated systems. Finally, in the last section, we briefly review the results of MC studies.

4.2 Geometrical frustration

Frustration may arise due to competing interactions in which various kinds of interfering interactions struggle to gain their own minimum energy. In this thesis we are interested in frustration caused by the lattice structure. We know that the ground

state (GS) of a ferromagnetic system establishes when all the spins are aligned. By contrast, for antiferromagnetic systems, the energetically favoured configuration is the one in which the neighboring spins are anti-aligned. Nevertheless, for some lattice structures, the optimal configuration is not the anti-aligned one. Examples of these lattice structures, which all contain elementary triangles, are triangular lattice, fcc lattice and hcp lattice. In these structures, one cannot have a GS in which all the interaction bonds between neighboring spins are fully satisfied.

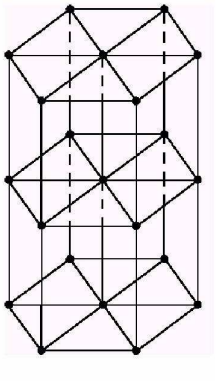

Figure 4.1: *hcp* structure of STA model

Some of the geometrically frustrated systems are:

4.2.1 Stacked triangular antiferromagnetic lattices

The first model to consider is the stacked triangular antiferromagnets (STA). Spins lie on stacked parallel layers that have hexagonal structure as shown in fig. 4.1. The Hamiltonian is

$$H = -\sum_{<ij>} J_{ij}\vec{S}_i \cdot \vec{S}_j \tag{4.1}$$

where J_{ij} are negative within the layers implying antiferromagnetic interactions. The J_{ij} are either negative or positive between the layers since no frustration arises along the direction of stacking (let us choose this direction as the z direction). In equation

(4.1), the $\vec{S}_i$ are n component spin vectors of unit length and the sum runs over all nearest neighbors. When $n = 1$, the Hamiltonian is that of one-component Ising spins. The situation is depicted in fig. 4.2 where the frustration arises because at least one of the interaction bonds is not satisfied. If $n = 2$, the Hamiltonian corresponds to XY system whose GS is shown in fig. 4.3. The GS is a planar non-collinear 120° structure of spins. Note, due to frustration, the spins are not anti-aligned. When $n = 3$, the Heisenberg case, the GS has the same structure, although the normal vector to the plane on which all spins lie can point in any direction.

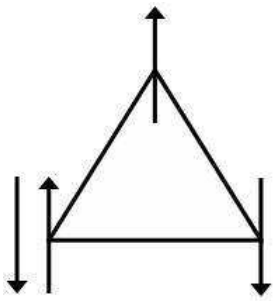

Figure 4.2: The GS configuration of three Ising spins on the corners of a triangle interacting antiferromagnetically. At least one of the interaction bonds is not satisfied no matter how the spins are arranged.

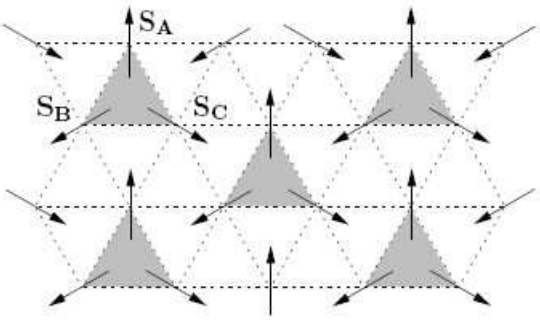

Figure 4.3: The GS configuration of XY and Heisenberg STA

The symmetry group of the Hamiltonian (4.1) is $O(n)$. Because of the non-collinear nature of GS, the symmetry breaks down to the $O(n-2)$ symmetry group which differs from the usual BS of non-frustrated systems. Hence the BS of the STA model is $O(n)/O(n-2)$. It can be written as $O(2)$ in the XY case and $SO(3)$ in the Heisenberg case.

4.2.2 STAR lattices

The stacked triangular antiferromagnetic lattices with rigidity (STAR) is a model almost the same as STA. In fact, it is derived from STA in this simple way: we can partition all the spins in the STA model into triangular cells of three spins called plaquettes. In fig. 4.3, the shaded triangles can be visualized as these plaquettes. It is worth to note that no spin is shared between plaquettes. Subsequently we impose a rigid constraint on each plaquette

$$\vec{S}_A + \vec{S}_B + \vec{S}_C = 0 \tag{4.2}$$

where A, B and C denote the spins on the corner of each plaquette. The constraint makes the spins on each plaquette rigidly fixed with respect to each other, however each plaquette is still free to rotate as a whole. This "constrained STA model" has the same ground state and BS as STA, so that we expect it to exhibit the same critical exponents and belong to the same universality class if it undergoes a second order phase transition. The expectation of having the same universality class may also be thought of in this way: by imposing the constraint, we only block the molecular-scale fluctuations which are irrelevant to the critical behavior. In other words, we only suppress the non-critical modes, so that we expect the critical behavior will not change.

4.2.3 Dihedral lattices

The dihedral lattices $V_{n,2}$ are derived from the STAR model. The geometry is similar to the STAR but, instead of plaquettes, we have spin pairs. Each spin pair is composed of two orthogonal spins denoted by e_1 and e_2. The Hamiltonian is written as

$$H = -J \sum_{<ij>} (e_1(i) \cdot e_1(j) + e_2(i) \cdot e_2(j)). \tag{4.3}$$

where J is positive implying ferromagnetic interaction. Equation (4.3) shows that e_1 (e_2) interacts only with e_1 (e_2). The GS of such a system is shown in fig. 4.4 which shows that all e_1 (e_2) are parallel at low temperature. The BS of this model is $O(n)/O(n-2)$ for n component e_i spins which is the same as the STA and STAR model.

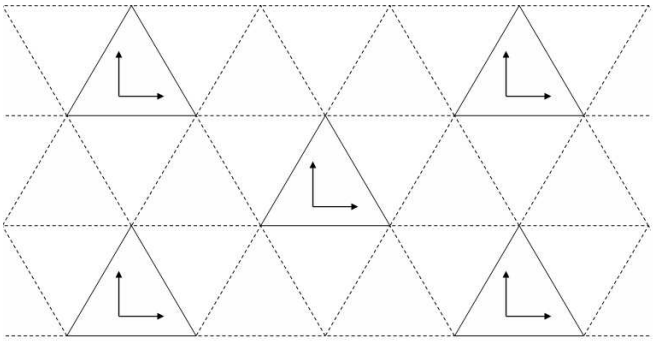

Figure 4.4: The GS configuration of the dihedral model

The continuum limit of the Hamiltonian (4.3) can be written

$$H = -\int d^d x [\partial e_1(x)]^2 + [\partial e_2(x)]^2. \tag{4.4}$$

The continuum limits are useful since renormalization group approaches usually work with the continuum limit of Hamiltonians.

4.3 Chiral universality class

The reader has noticed that the BS for all of the models mentioned in the previous section is $O(n)/O(n-2)$. This BS is a consequence of the non-collinear structure of the GS and naturally differs from the BS of non-frustrated systems which is $O(n)/O(n-1)$. We already found that the concept of BS plays an important role in determination of the universality class of each system. In fact, the BS in frustrated spin systems is more complicated than non-frustrated ones, and so is the nature of the phase transition. It is believed that if the phase transition in frustrated spin systems is second order, then they should belong to a new universality class called the chiral universality class.

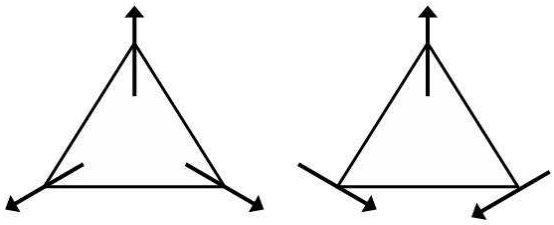

Figure 4.5: The chiral degrees of freedom in ground state of STA and STAR

Another way to anticipate the existence of the chiral universality class is the appearance of new chiral degrees of freedom. The idea was first proposed by Kawamura [18] and then received support from MC simulations. There is a two fold degeneracy associated with the 120° structure of STA and STAR model as shown in fig. 4.5. In order to describe this degeneracy, we may define a vector called chirality as follows

$$\vec{k} = \frac{2}{3\sqrt{3}}[\vec{S}_A \times \vec{S}_B + \vec{S}_B \times \vec{S}_C + \vec{S}_C \times \vec{S}_A] \tag{4.5}$$

where $\vec{S}_A$, $\vec{S}_B$ and $\vec{S}_C$ are the spins on the corners of a plaquette. The chirality is only defined for systems with non-collinear GS. For XY systems, the chirality has only a component in the z direction. As shown in fig. 4.6, it assigns a chiral value of either +1 or -1 to each triangle in the GS which resembles the Ising ordering. So

the chirality has an Ising symmetry. This symmetry along with the $SO(2)$ rotational symmetry of spins in the xy plane means that the order parameter space is described by $Z_2 \times SO(2) = O(2)$ BS. For Heisenberg systems, however, the chirality has three components since the normal to the spin plane can be in any direction.

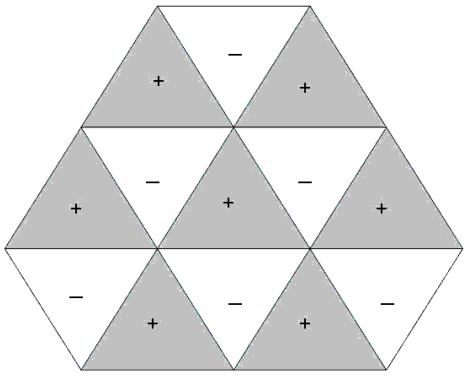

Figure 4.6: The chirality values assigned to each triangle

Finally, it is worth to remark that the $O(n)/O(n-2)$ BS is the most important BS for frustrated systems, but it is not the only one. For example, the existence of next-nearest-neighbor interactions usually changes the BS as the system remains frustrated. In addition, one needs to consider the uncommon phenomena of reduction in lattice symmetries. So we can generalize all the BS of frustrated systems as $S_{lattice} \otimes \ O(n)/O(n-P)$ where $S_{lattice}$ accounts for the possible reduction of the lattice symmetries and P varies from 1 to n [19].

4.4 The experimental situation

There have been several experimental studies of frustrated magnets on a rich variety of materials. The most well-known materials with STA structure are the ABX_3-type compounds where A is an alkali element such as Cs or Rb, B is a magnetic ion such as Mn, Ni or Co, and C corresponds to halogens such as Cl, Br and I. VCl_2 and

VBr_2 are also believed to share the same structure too. Almost all of the experimental studies have reported a second order phase transition. However, universality is often violated since critical exponents vary from one material to another. This non-universal behavior is not consistent with our current picture of critical phenomena.

An important issue dealing with these materials is the presence of magnetic anisotropies. Anisotropy destroys the rotational symmetry of Heisenberg spin systems and as a result changes the critical behavior associated with them. The planar or axial anisotropies cause a succession of crossovers from Heisenberg to Ising or XY behavior which leads to some difficulties in the interpretation of the data. In fact, this is the reason why we have a richer experimental situation for XY frustrated systems. Some of the critical exponents for the XY STA compounds are summarized in Table 4.1. The most well-known compound of this type, studied by magnetic neutron scattering and specific heat measurements, is $CsMnBr_3$ which exhibits a second order phase transition with critical exponents compatible with the MC calculations. An exception to this critical behavior is the anomalous critical behavior of $CsCuCl_3$ whose specific heat exhibits a crossover from the chiral XY exponent $\alpha \approx 0.35$ to a first order behavior very close to T_c [20].

The situation is more complicated for the study of Heisenberg systems since there is no pure Heisenberg compound. VCl_2, VBr_2 and $RbNiCl_3$ are nearly Heisenberg systems due to presence of weak axial anisotropies. Fortunately, for a few materials such as $CsNiCl_3$, we are able to obtain Heisenberg-like magnets from Ising-like magnets by the use of an external magnetic field of appropriate intensity to counterbalance the axial anisotropy. Table 4.2 gives a summary of critical exponents for different materials that are believed to be Heisenberg STA materials. Delamotte et al. [31] categorized these materials into two groups according to their corresponding critical exponents. One group (group 1) is consistent with the existence of a chiral universality class due to compatibility of its exponents with the MC results. The scaling relations are satisfied and the anomalous dimension η is marginally negative.

Materials	Ref.	α	β	γ	ν
$CsMnBr_3$	[21]		0.24(2)		
	[22]		0.22(2)		
	[23]		0.25(1)		
	[24]		0.21(2)	1.01(8)	0.54(3)
	[25]	0.39(9)			
	[26]	0.40(5)			
	[26]	0.44(5)			
	[27]			1.10(5)	0.57(3)
$CsNiCl_3$	[28]	0.37(8)			
	[28]	0.37(6)			
	[29]	0.342(5)			
	[30]		0.243(5)		
$CsMnI_3$	[28]	0.34(6)			
$CsCuCl_3$	[20]	0.35(5)	*first order*		

Table 4.1: The critical exponents of XY STA materials

By contrast, for the other group (group 2), the scaling relations are violated and the anomalous dimension is more negative. Actually, there is axial anisotropy involved in the study of the materials of group 2. So one may argue that violation of universality here is not important because we should not expect the materials of group 2 to belong to the same universality class as the group one at all. In other words, maybe the group 2 cannot be described by a Heisenberg spin system.

Materials	ref.	α	β	γ	ν	group
VCl_2	[32]		0.20(2)	1.05(3)	0.62(5)	2
VBr_2	[33]	0.30(5)				2
$RbNiCl_3$	[34]		0.27(1),0.28(1)			1
$CsNiCl_3$	[28]	0.25(8)				1
	[29]	0.23(4)				
	[30]		0.28(3)			
$CsMnI_3$	[28]	0.28(6)				1
$CuFuD$	[35]		0.22(2)			2

Table 4.2: The critical exponents of materials that are believed to correspond to Heisenberg STA

4.5 Renormalization Group

As we discussed previously, the critical behavior only depends on the spatial dimension d and BS. We focus here on the $O(n)/O(n-2)$ BS. It is expected that the critical behaviors of the models with this BS (STA, STAR, ...) are equivalent, however it seems that the situation is more complicated. To investigate the situation from a theoretical point of view, we use the renormalization group (RG) analysis. RG analysis has contributed significantly to our understanding of critical phenomena. It has also revealed some interesting results in studying the peculiar behavior of frustrated systems in their critical region.

RG is basically a consequence of the Kadanoff picture of the critical region [36]. We divide the lattice sites into blocks, and then replace each block by only one

site. The transformation is called the renormalization transformation. After each renormalization transformation we define a new effective Hamiltonian for the system which has the same form as the original one but with different parameters. The successive use of the renormalization transformation will introduce a flow of "the effective parameters" toward (and away from) some special points called *fixed points*. A fixed point is a point in parameter space which is mapped onto itself by the use of renormalization transformation. Fixed points are classified as being attractive, repulsive, or mixed according to the flow direction of the effective parameters in their neighborhood. The existence of a nontrivial fixed point implies the divergence of correlation length and thus a second order phase transition.

The scheme of RG which has been applied to frustrated systems is the field theoretical renormalization group scheme. It has given elegant results for the systems with the $O(n)/O(n-1)$ BS which belong to the so-called Wilson-Fisher universality class. The success of the field theoretical RG scheme in describing these systems is due to the fact that $O(n)$ symmetry group corresponds to the maximal symmetry and there is only one coupling constant and as a result only one nontrivial fixed point. However, for frustrated systems (such as the STA and dihedral model), the different approaches of the field theoretical RG scheme have come to different conclusions. This is the topic of this section to briefly discuss different formulations of the field theoretical RG and their conclusions to our problem. In general, the field theoretical RG analysis is based on three main approaches:

4.5.1 The Landau-Ginzburg-Wilson (LGW) model approach

With the Hamiltonian of interactions between classical spins, we implicitly assume one constraint that the spins are of fixed length. However, for our convenience, we often replace the constraint with a less strict one. This is the first step to describe the Landau-Ginzburg-Wilson (LGW) model approach. Then we transfer the Hamiltonian from the position space to the wave vector space by performing a Fourier transform

and remove the non-critical modes (large wave vectors or short wavelengths) of the order parameter. At the end, we have a Hamiltonian expanded in terms of the order-parameter fields. The LGW Hamiltonian for ferromagnets is the famous ϕ^4 model and is given by

$$H = \int d^d x[(\nabla\phi)^2 + r\phi^2 + u\phi^4] \tag{4.6}$$

where d is the dimension of the system and ϕ is the n-component order-parameter field. Nevertheless, in the case of non-collinear structures, two equivalent vector fields similar to what we have in the dihedral model are needed. The Hamiltonian [37, 38] is

$$H = \int d^d x[(\nabla\phi_1)^2 + (\nabla\phi_2)^2 + r(\phi_1^2 + \phi_2^2) + u(\phi_1^2 + \phi_2^2)^2 + v((\phi_1 \cdot \phi_2)^2 - \phi_1^2\phi_2^2)] \tag{4.7}$$

where v should be a positive scalar in order to represent a non-collinear GS. If $v < 0$, the two vector fields do not favor an mutually orthogonal structure. This Hamiltonian is used for some of the RG analyses such as the $\epsilon = 4-d$, $1/n$, and RG loop expansion.

In general, using the $\epsilon = 4 - d$ expansion, four possible fixed points are found. Only two of these points correspond to the non-collinear nature of the GS, and just one of these two is the stable fixed point which implies the existence of a chiral universality class. Generally the presence of this fixed point in real parameter space depends upon the number of spin components. In fact there is a critical value of the number of spin components n_c such that if $n > n_c$, the phase transition is of second order. For $n < n_c$, the two fixed point move to the complex parameter space and as a result a first order transition is expected. This critical value must be compared to physically important values of $n = 2$ and $n = 3$. In 1988, Kawamura found [37]

$$n_c(d = 4 - \epsilon) = 21.8 - 23.4\,\epsilon + O(\epsilon^2), \tag{4.8}$$

so, on the basis of his MC simulation, he concluded a second order phase transition for $d = 3$. He also performed $1/n$ expansion and found second order transition for $2 < d < 4$ with the exponents consistent with ϵ-expansion results. However, in

1995, higher order calculations to $O(\epsilon^3)$ performed by Antonenko *et al.* [39] resulted in the value $n_c(d = 3) = 3.39$ which implies a first order transition. The same authors also used a three loop order LGW analysis directly in $d = 3$ [40] and found $n_c(d = 3) = 3.91$. In the same year, a modified version of $1/n$ expansion [41] was also employed and led to a second order transition in $d = 3$ for $n = 2$ and $n = 3$. In 2001, Pelissetto *et al.* [42] showed the existence of a stable fixed point for $n = 2$ and $n = 3$ exploiting a six loop series for the LGW model. Subsequently, in 2002, Calabrese *et al.* [43] by using almost the same scheme as Pelissetto up to six-loop expansion found evidence of the existence of a stable fixed point. They argued that the non-universal behavior associated with the different experimental and computational results might be due to unusual spiral-like approach to the fixed point. In 2004, Calabrese *et al.* [44], using a five loop series but a different scheme of LGW called Minimal-Subtraction scheme without ϵ expansion, came to the same conclusion as the group's previous result.

In general, the LGW approaches favor a second order phase transition. The LGW approach, as is the $NL\sigma$ approach that is the topic of the next subsection, are perturbative approaches in a sense that they are expansions in terms of the dimension or the coupling constants. Later on, we will see that there exist non-perturbative approaches that lead to contradictory results with respect to the LGW approaches.

4.5.2 The $NL\sigma$ model approach

$NL\sigma$ approach relies on an expansion about $d = 2$ and also about low temperature where the symmetry is broken. In contrast to the LGW approach, the length of spins are fixed. The $NL\sigma$ accounts for the critical fluctuations of the system as it gains more thermal energy. Azaria *et al.* [45] applied this approach to study the case $n = 3$ specifically and then generalized it to any $O(n)/O(n-2)$ BS. For $n = 3$, they found a fixed point which surprisingly corresponds to an enlarged $SO(4)/SO(3)$ BS. It means that it is a Wilson-Fisher fixed point for $n = 4$. They further stated that the fixed

point could also be first order or mean-field tricritical, depending on the microscopic parameters of the system. However neither the numerical nor experimental studies agree with a Wilson-Fisher behavior of $n = 4$ or a mean-field tricritical behavior.

4.5.3 The non-perturbative approach

The non-perturbative RG (NPRG) approach based on the idea of blocking the spins and coarse-graining has also been used for the study of critical phenomena. Zumbach [46] performed the first NPRG approach to frustrated magnets in 1993. By using a local potential approximation, he found $n_c = 4.7$ which implies a first order transition for $n = 2$ and $n = 3$. The important conclusion of his study, though, was the existence of a minimum of flow in RG flow for $n = 3$ as a consequence of the appearance of two complex fixed points. He interpreted that this minimum simulates a fixed point that is, in fact, a pseudo-fixed point and as a result scaling behavior can be observed. However, no minimum of flow was found for $n = 2$ whereas the scaling was already seen in the experimental and numerical studies.

Following Zumbach, Delamotte et al. [47, 48] argued that a minimum of flow is neither a necessary nor sufficient condition to justify the pseudoscaling. Using the technique of effective average action, they found $n_c = 5.1$. They explained the occurrence of scaling for $n = 2$ and $n = 3$ without universality as a result of a whole region in parameter space where the RG flow is very slow as shown in fig. 4.7. They also claimed that all known perturbative results at one-loop in two and four dimension were recovered.

4.6 Numerical situation

The critical exponents for some Heisenberg frustrated systems obtained by MC simulation are summarized in Table 4.3. Generally speaking, for the STA model, the idea of the existence of the chiral universality class was supported since a second or-

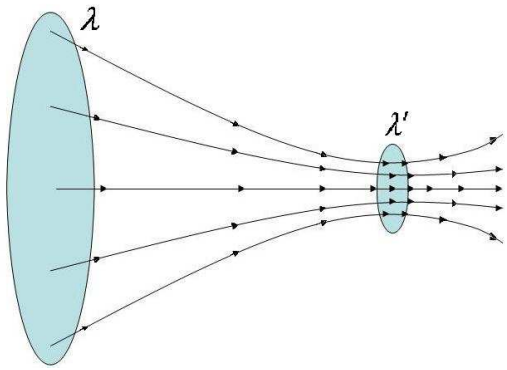

Figure 4.7: The RG flow from the coupling constant region λ to the coupling constant region λ'. All the trajectories are attracted to λ' where the RG flow is slow.

der phase transition with new critical exponents was found. However, some of these studies have resulted in negative values for anomalous dimension η. A negative value of η is unexpected since it is already proved for some models such as ϕ^4 that $\eta \geqslant 0$ [49]. The physical meaning of this is that the fluctuations should lead to decrease the correlation of the system with the spatial distance according to the equation (2.10).

The non-universal behavior of these systems from a computational point of view was revealed by Dorby and Diep [50] who studied the STAR model and found clearly different exponents from STA. Later on, Loison et al. [51] investigated the same model more precisely and also found distinct exponents from STA. The value of η was found to be even more negative than that of STA and, in fact based on this, Loison et al. concluded a first order phase transition. In addition, they examined the dihedral model and obtained rather consistent exponents with those of STAR, but not STA [51]. The variation in the values of the critical exponents is inconsistent with the universality of a second order phase transition since the transitions with the same BS are expected to exhibit the same critical behavior.

It should be noted that there has been a Monte Carlo Renormalization Group (MCRG) study of frustrated magnets by Itakura [56]. He studied the STA and dihe-

Models	ref.	α	β	γ	ν
STA	[52]	0.240(80)	0.300(20)	1.170(70)	0.590(20)
	[53]	0.242(24)	0.285(11)	1.185(3)	0.586(8)
	[54]	0.245(27)	0.289(15)	1.176(26)	0.585(9)
	[55]	0.230(30)	0.280(15)		0.590(10)
STAR	[51]	0.488(30)	0.221(9)	1.074(29)	0.504(10)
Dihedral	[51]	0.479(24)	0.193(4)	1.136(23)	0.507(8)

Table 4.3: The critical exponents of Heisenberg frustrated magnets calculated by Monte Carlo simulations

dral model in order to get their corresponding RG flow digram. He found $3 < n_c < 8$, so concluded a first order phase transition for the physically interesting number of components. He also performed MC calculations of the XY and the Heisenberg STA model and found a first order transition only for the XY STA system, consistent with the MCRG study. He then argued that a larger system size is needed in order to expose the first order behavior of the Heisenberg STA.

Chapter 5

SHORT TIME DYNAMICS

5.1 Introduction

Systems that undergo a second order phase transition have been known for a long time to exhibit a scaling behavior in equilibrium. We have already seen that the scaling behavior leads to the power law behavior in some of the properties of the system as a function of the reduced temperature. However, a new type of scaling behavior was found recently to be valid for such systems even if they are far from equilibrium. In contrast to the equilibrium scaling form, the "non-equilibrium" scaling behavior leads to the power law behavior of some quantities as a function of *time*. The method of exploiting this scaling behavior is called the *short time dynamics* method and is the subject of this chapter. First we introduce the general scaling form and then we discuss its consequences that enable us to measure the static critical exponents as well as the dynamic critical exponent z.

5.2 General scaling form

In 1989, Janssen et al. [57] showed that the universal behavior of a system with $O(n)$ symmetry can already be observed during the relaxation process of the system far from equilibrium. Using a renormalization group approach, they introduced a scaling form for the k-th moment of the magnetization as follows

$$m^{(k)}(t, \tau, L, m_0) = b^{-k\beta/\nu} m^{(k)}(b^{-z}t, b^{1/\nu}\tau, b^{-1}L, b^{x_0}m_0) \tag{5.1}$$

where L is the linear lattice size, t is the time, b is an arbitrary scaling factor and τ is the reduced temperature defined by

$$\tau = \frac{T - T_c}{T_c}. \tag{5.2}$$

In equation (5.1), m_0 is the initial value of the order parameter of the system and x_0 is a new exponent associated with the scaling of the initial magnetization. In order to observe the critical relaxation, one can initialize the system either in a completely ordered state corresponding to $T = 0$ or in a disordered state corresponding to high temperature configuration, and then quench the system to T_c. The scaling behavior emerges after a microscopic time scale t_{min} which is much smaller than the time to reach the equilibrium. The scaling form is only valid in an intermediate time interval from t_{min} until a maximum time at which the system is still sufficiently far away from the long-time behavior. This intermediate time interval is called short-time region.

5.3 How do we exploit the scaling form?

If we choose the scaling factor $b = t^{1/z}$, the right side of equation (5.1) for the first moment of the order parameter is written as

$$m(t, \tau, m_0) = t^{-\beta/\nu z} m(1, t^{1/\nu z}\tau, t^{x_0/z} m_0). \tag{5.3}$$

For $m_0 << 1$ which implies a disordered configuration start, we may expand equation (5.3) as follows

$$m(t, \tau, m_0) \sim m_0 t^{(x_0 - \beta/\nu)/z} F(t^{1/\nu z}\tau) + O(t^{x_0/z} m_0]^2) \tag{5.4}$$

where the fact that $m(t, \tau, m_0 = 0) = 0$ has been used. Exactly at the critical temperature ($\tau = 0$), the scaling form of equation (5.6) reduces to a power law behavior as follows

$$m(t) \sim t^{\theta} \tag{5.5}$$

where a new exponent $\theta = (x_0 - \beta/\nu)/z$ has been introduced. For temperatures close to T_c, the power law behavior is modified by the scaling function F, so that a good power law behavior can not be obtained.

Note that in this calculation we implicitly assumed that there is no L dependence. This is a reasonable assumption as long as the system size is sufficiently large and the correlation length is sufficiently small. For the second moment of magnetization, however, there is an intrinsic L dependence even if the correlation length is small. At high temperature, as a matter of fact we have $m^{(2)} \sim L^{-d}$. This leads to the power law behavior for the second moment of magnetization as

$$m^{(2)}(t) \sim t^{(d-2\beta/\nu)/z}. \tag{5.6}$$

From the general scaling form, again choosing $b = t^{1/z}$, one can also derive the following expression

$$\partial_\tau \ln m(t,\tau)|_{\tau=0} \sim t^{1/\nu z} \tag{5.7}$$

which allows us to obtain the ratio $1/\nu z$.

The above equations are valid for a disordered configuration start. However, the scaling relations for an ordered configuration start are rather different since the initial value of the order parameter $m_0 = 1$. In fact, for a low temperature start, the general scaling reduces to

$$m^{(k)}(t,\tau,L) = b^{-k\beta/\nu} m^{(k)}(b^{-z}t, b^{1/\nu}\tau, b^{-1}L) \tag{5.8}$$

where the m_0 dependence of the general scaling form was excluded. This leads to the derivation of the short-time scaling relations for the first and second moment of the order parameter as follows

$$m(t) \sim t^{-\beta/\nu z} \tag{5.9}$$

$$m^{(2)}(t) \sim t^{-2\beta/\nu z}. \tag{5.10}$$

In addition, a Binder cumulant can be defined [58] which behaves as follows

$$U(t) = \frac{m^{(2)}}{(m)^2} - 1 \sim t^{d/z}. \tag{5.11}$$

The existence of this quantity is important since it enables us to estimate the dynamic exponent z directly, independent of other static exponents. Equation (5.7) is also valid for an ordered configuration start, so the same equation can be used to determine the exponent $1/\nu z$ for both cases of the initial configuration.

5.4 Monte Carlo simulation of short-time dynamics

In chapter 3 we pointed out the problem of critical slowing down which requires long simulation times near the critical temperature. The problem is simply due to the large value of the correlation time once the system is in equilibrium. As a consequence, one needs to update the system for so many times in order to obtain a new independent microstate. Some cluster algorithms were suggested [7, 8] and, in fact, found useful to remove or considerably reduce the problem. However, they are only applicable to some special systems such as Ising model. An alternative method that is free of critical slowing down is the short time dynamics method. It provides a technique to calculate the critical temperature and critical exponents of different systems when they are far from equilibrium. Since the system is not in equilibrium, the correlation length is small and the critical slowing down is absent. This is a remarkable advantage because we do not need to perform a huge number of MC steps.

The time unit in MC simulation is a MC time step (mcs) at which all spins in the system are updated or at least given the chance to update once. In the equilibrium MC simulation, one averages over the values of the quantity of interest at different times. In the short-time region MC simulation, however, the average is performed over different samples at the same time. In other words, because a single run would lead to noisy data, we have to make equivalent runs for different samples. We mean different samples in the sense that the samples are updated by different random number sequences.

5.5 First order vs second order short time behavior

The short time dynamic approach works due to the existence of a large correlation time which brings on a memory effect [59]. This memory effect causes the scaling behavior in the short time region of a system undergoing a second order phase transition. For a first order phase transition, the correlation time is not large and as a result there is no scaling behavior. However, if it is a weak first order transition, the correlation time might become large enough such that a scaling behavior can be seen. In such a case, one needs to use special techniques in order to distinguish the order of the transition.

One technique can be the use of the concept of metastability. We know that, for a fist order transition, there exists a disordered metastable state in a small temperature range below the transition temperature T_t. The state disappears at the temperature T_{t1}. Similarly there is an ordered metastable state in a temperature range above T_t which disappears at the temperature T_{t2}. The relation $T_{t1} < T_t < T_{t2}$ is always true for a first order phase transition. For a second order phase transition, however, there is no metastability and we have $T_{t1} = T_{t2} = T_c$. With this knowledge, we can perform the simulation for both initial configurations to measure the transition temperatures associated with them. Then, we look for the metastability in order to distinguish the order of phase transition. A second order phase transition will be concluded if no metastability is detected. In an article by Schulke and Zheng [60], the technique was introduced and used to investigate the order of the phase transition in the Potts model. They showed the apparent existence of the metastability for the five and seven-state Potts model which led them to conclude a first order phase transition.

Chapter 6

A FAMILY OF HEISENBERG NON-COLLINEAR MAGNETS

6.1 Introduction

In chapter 4, we reviewed some of the studies on frustrated spin systems. From the numerical point of view, the STA and STAR models which share the same BS were found to exhibit different critical behavior [50, 51]. This non-universal behavior is inconsistent with a second order phase transition. So far there has been no general agreement on the nature of the phase transition associated with these systems. The question arises whether this means that the critical behavior depends on the microscopic details of the interactions between particles and, as a result, the phase transition is first order. In particular, one is also interested to see how the "rigidity constraint" of the STAR model affects the critical behavior. The aim of this chapter is to investigate frustrated systems of this type and provide insight into the understanding of the nature of the phase transition associated with them.

This chapter is organized as follows: first we introduce a model which represents a family of Heisenberg non-collinear magnets. Then we describe the method of calculations using the short-time dynamics approach. Afterwards, we will discuss the results for two initial configurations: an ordered and disordered configuration. Finally we will consider a modified method for the short-time dynamics study of the STAR model.

6.2 Model and Method

In order to examine the effect of the local rigidity on STAR, it is interesting to provide a situation in which one can reach the STAR model from the STA model in a smooth manner, so that one can see how the critical behavior changes. This can be accomplished by introducing the following Hamiltonian

$$H = -\sum_{<ij>} J_{ij}\vec{S}_i \cdot \vec{S}_j + r \sum_{plaquettes} (\vec{S}_A + \vec{S}_B + \vec{S}_C)^2 \tag{6.1}$$

where the first part of the Hamiltonian is the STA model. Needless to say that the geometry is the same as STA geometry. In equation (6.1), $\vec{S}_A$, $\vec{S}_B$ and $\vec{S}_C$ denote the spins on the corners of each plaquette and the sum in the second part runs over all plaquettes. The main point is the introduction of the parameter r which is called the constraint parameter. The case $r = 0$ corresponds to STA and as r increases toward $r = \infty$, we reach the STAR limit. However, as we will see shortly, the constraint parameter is more useful than just tuning between the STA and STAR models. This Hamiltonian has been used previously to study the case of XY frustrated systems [61, 62].

To see how the constraint parameter changes the local rigidity, it is convenient to expand the last term. For each plaquette, we have

$$(\vec{S}_A + \vec{S}_B + \vec{S}_C)^2 = \vec{S}_A^2 + \vec{S}_B^2 + \vec{S}_C^2 + 2\vec{S}_A \cdot \vec{S}_B + 2\vec{S}_B \cdot \vec{S}_C + 2\vec{S}_A \cdot \vec{S}_C \tag{6.2}$$

The $\vec{S}^2$ terms are constants and can be ignored. Hence the Hamiltonian (6.1) is equivalent to

$$H = -\sum_{out} J_{ij}\vec{S}_i \cdot \vec{S}_j - \sum_{in}(J_{ij} - 2r)\vec{S}_i \cdot \vec{S}_j \tag{6.3}$$

where $\sum_{in}$ sums over all the interactions of spins inside the plaquettes and $\sum_{out}$ sums over all the interactions of spins connecting different plaquettes.

One notices that the effective interaction constant between the spins of each plaquette is $(J_{ij} - 2r)$. Since $J_{ij} < 0$, as r increases from zero, the antiferromagnetic

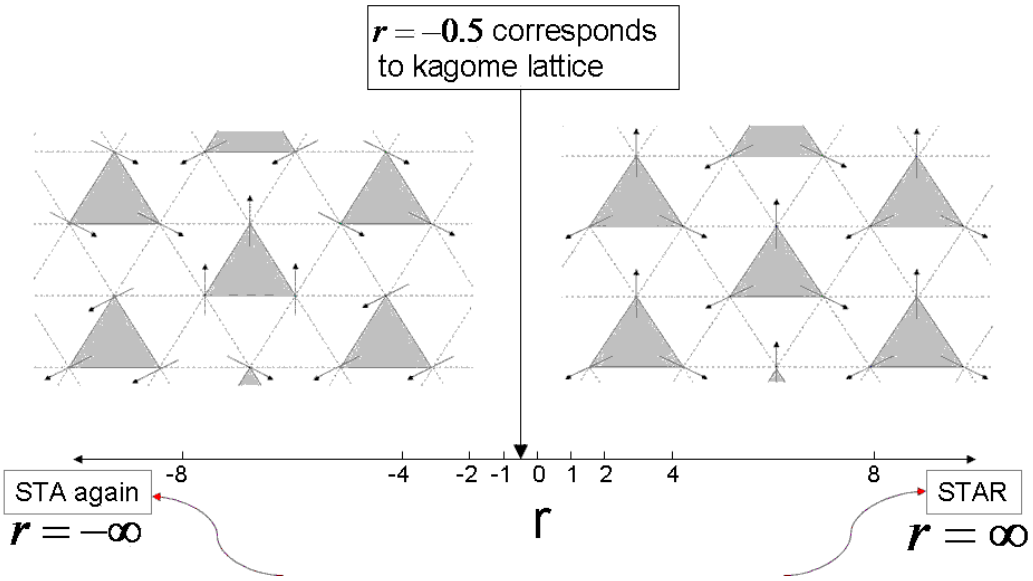

Figure 6.1: On either side of $r = -0.5$, the structure of the corresponding GS are shown. These two GS are degenerate exactly at $r = -0.5$.

interaction inside each plaquette becomes stronger such that, in the $r = \infty$ limit, the spins in one plaquette are rigidly fixed in a 120° structure with respect to each other. The structure of the GS remains the same as the constraint parameter is varied in this range of values. The case of the STAR model is one in which plaquettes are free to rotate as a whole but constrained to have locked spins within. The right side of fig. 6.1 shows the structure of the GS for positive r.

This is not the end of story as some of the interesting consequences of the generalized Hamiltonian arise when r is negative. This range has not been studied previously in the XY case. Without loss of generality, we take the interaction constant within triangular planes to have the value $J_{ij} = -1$, so that $-1 + 2r$ will be the interaction constant within the plaquettes. If $r < -0.5$, the spins in each plaquette interact ferromagnetically and favor a parallel configuration with respect to each other. The left side of fig. 6.1 shows the GS applicable to such a system. Since the interactions among plaquettes remain antiferromagnetic ($J_{ij} = -1$), each plaquette orients in

$\pm 120^\circ$ angle with respect to the neighboring plaquettes. Therefore the non-collinear nature of the system is preserved.

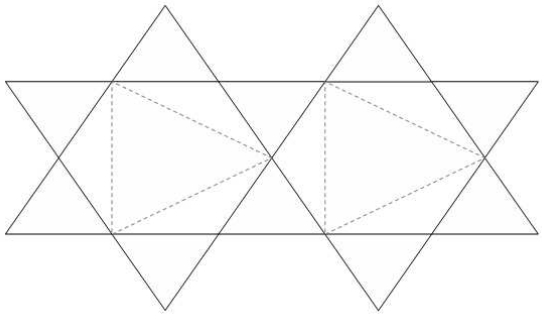

Figure 6.2: The geometry of the Kagome lattice in $d = 2$. The dashed lines indicate the interactions which vanish at $r = -0.5$

There are four important, "critical" values of r. We already discussed two of them ($r = \infty$ and $r = 0$). The other two are the following:

- $r = -0.5$ implies that $(J_{ij} - 2r) = 0$. This means that there is no interaction between the spins in each plaquette. As a result, every spin has only four neighbors in the plane and the geometry is the same as a system of stacked Kagome layers. The geometry of each Kagome layer is shown in fig. 6.2. This system is known to possess a highly degenerate GS [63]. The two GS shown in fig. 6.1 are degenerate exactly at $r = -0.5$.

- For $r = -\infty$, spins on each plaquette point in the same direction at all temperatures. One only needs to know the direction of one spin in order to specify the directions of the other two in the plaquette. In other words, we can replace each plaquette by one *block spin*. By doing so, the GS of the block spins remains the same as that of the STA model. Hence one concludes that the $r = -\infty$ limit also corresponds to the STA model.

Regarding these "critical" values of r, we partition the model into three distinct cases. One case is near $r = -0.5$ denoted by $(-1, 0)$. This small range is influenced by the highly degenerate Kagome structure at $r = -0.5$. This case itself is composed of two ranges $(-1, -0.5)$ and $(-0.5, 0)$ which have distinct GS. It is not the goal of this thesis to examine the case $(-1, 0)$ in detail, however we will comment on some of the interesting points later on. The other r cases are $[-\infty, -1]$ and $[0, \infty]$. In the next section, we will discuss these two latter cases.

We have used the short-time dynamics approach to determine the critical temperatures and critical exponents for various fixed values of r. We prepare the system either in a completely ordered state or in a disordered state, and then we quench the system to a number of temperatures close to the expected T_c. As a result of the quenching, the system evolves towards the new equilibrium. In order to exploit the scaling relations of chapter 5, we follow the order parameter as a function of time t using a heat-bath algorithm to update the system.

Using the relaxation curves for different temperatures, we look for the temperature which has the best power law behavior. This temperature corresponds to the critical temperature T_c. This can be done by interpolation: we interpolate the relaxation curves for a number of intermediate temperatures. For perfect power law behavior, the log-log plot of the order parameter versus time is a straight line with a slope that is equal to the exponent. Hence searching for the best power law reduces to searching for the best straight line. We fit a straight line to the $\log m$ versus $\log t$ using a least-square method, and then we calculate the goodness of the fit. The temperature which possesses the maximum goodness will be the T_c.

It is worth to note that, for large values of $|r|$, the spins of each plaquette are effectively locked together. A single-spin flip algorithm is not efficient for these values of r. If one is interested in large values of r, one should modify the algorithm to update the whole plaquette simultaneously rather than just one of its spins.

6.3 Results and Discussion

6.3.1 Ordered configuration start

An ordered configuration state corresponds to the zero temperature GS where the order parameter has its maximum value. For $r > -0.5$, there are three sublattices each of which has all its spins parallel in the GS. The initial configuration of spins at $t_0 = 0$ for these sublattices can be chosen as follows:

$$\vec{S}_A = \hat{i}$$

$$\vec{S}_B = (-\hat{i} + \sqrt{3}\hat{j})/2 \tag{6.4}$$

$$\vec{S}_C = (-\hat{i} - \sqrt{3}\hat{j})/2.$$

where $\hat{i}$ and $\hat{j}$ are the unit vectors along the x and y directions. It should be noted that the structures of three sublattices are different for $r < -0.5$. In the $r < -0.5$ case, the spins of each plaquette belong to one sublattice. However, the plaquettes form three sublattices which can also be labeled as A, B, C.

The components of the magnetization for the three sublattices are defined as follows

$$m_{\alpha\beta} = \frac{3}{N} \sum_{i=1}^{N/3} S_{i\beta}^{\alpha} \tag{6.5}$$

where $\alpha = A, B, C$, $\beta = x, y, z$ and N is the total number of spins in the system. At t_0, the magnetization components are

$$m_{Ax}^0 = 1$$

$$m_{Bx}^0 = m_{Cx}^0 = -0.5 \tag{6.6}$$

$$m_{By}^0 = -m_{Cy}^0 = \sqrt{3}/2,$$

and zero for the rest of the components. The relaxation process can only be observed for the components which are set non-zero initially. Fig. 6.3 shows a schematic view

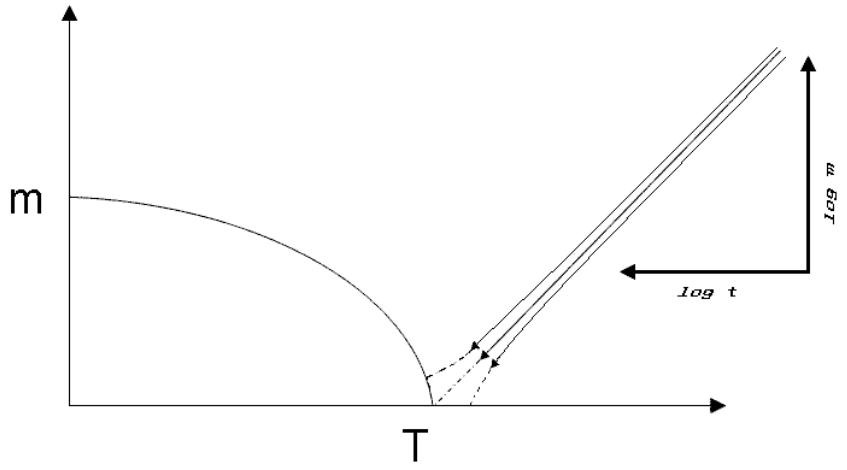

Figure 6.3: A schematic view of the logarithmic scaling behavior of m as a function of t. Only for T_c, the order parameter follows a power law type path in order to relax toward the equilibrium. For a temperature close to T_c, the power law behavior is modified according to the value of τ

of the short-time scaling behavior. At T_c, the order parameter follows a power law type path in order to relax toward the equilibrium. For a temperature close to T_c, the power law behavior is modified according to the value of τ. For $\tau > 0$, the order parameter relaxes towards zero whereas, for $\tau < 0$, it relaxes towards a finite value. In fig. 6.4, we show the order parameter curves m_{Ax} versus t on a log-log scale for three quenched temperatures with $r = 1$. Interpolation of the data is performed to find the best power law behavior which corresponds to T_c. The figure demonstrates how the behavior of the order parameter as a function of t deviates from a straight line for temperatures close to T_c in a typical case. In the upper curve, the temperature is below T_c and the slope of the relaxation decreases. The lower curve, however, corresponds to a temperature above T_c. One sees that the slope of the relaxation increases in this case. The solid line is the interpolated curve which yields the best power aw behavior and therefore corresponds to T_c.

In fig. 6.4, the relaxation curves of the three chosen temperatures are too dis-

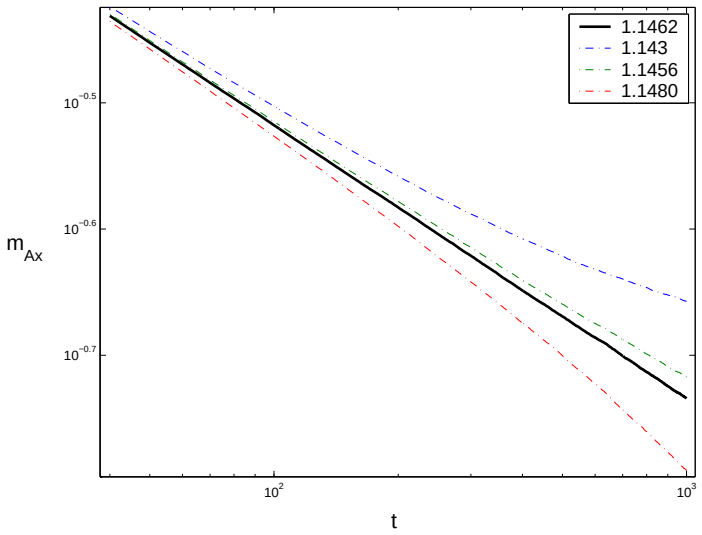

Figure 6.4: The order parameter curve versus t on a log-log scale for three quenched temperatures and $r = 1$. The solid line represents the interpolated curve which yields the best power law behavior

persed. This reduces the accuracy of interpolations and, as a result, the accuracy of final results. In addition, to find a good estimate of $\partial_\tau \ln m(t,\tau)|_{\tau=0}$, one needs smaller differences in the temperatures. To do so, we attempt to select temperatures that are closer to each other as well as to T_c. This makes the interpolation much more accurate. As an example, we show the relaxation curves of m_{Ax} along with the corresponding log-log plot for $r = 0$ in figure 6.5. One sees that the order parameter curves of different temperatures are so close that it is hard to distinguish them. We will show shortly how we make sure that the T_c falls in this small temperature range.

An important part of the procedure to obtain the best fit is to estimate t_{min}, the time at which the scaling behavior appears. To estimate t_{min}, we divide the available time range into intervals of size l (mcs). Then we calculate the exponent associated with the order parameter in each time interval. We shall refer to the exponent of each time interval as the local exponent of the interval. Needless to say that, for an ordered configuration state, the exponent is $\beta/\nu z$. Before t_{min}, the local exponents change as

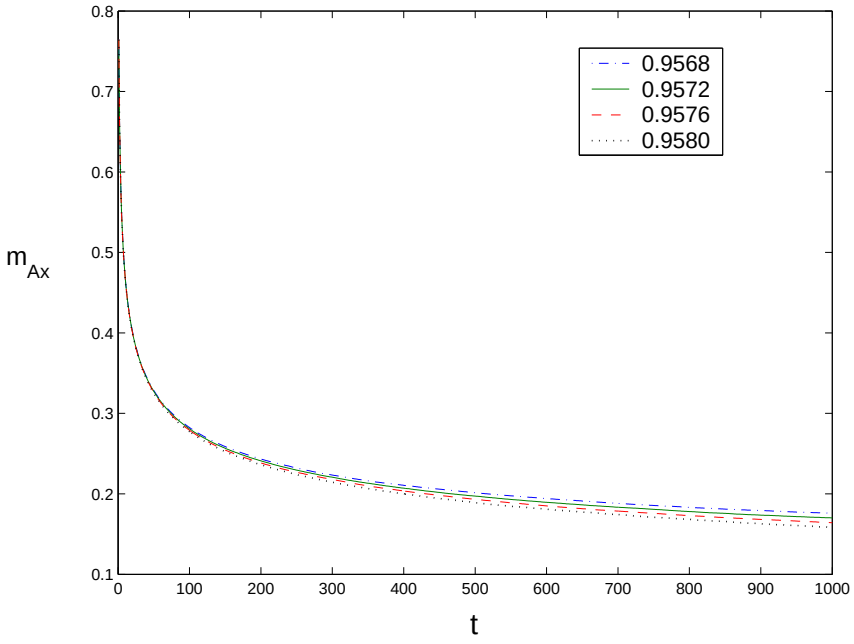

(a)

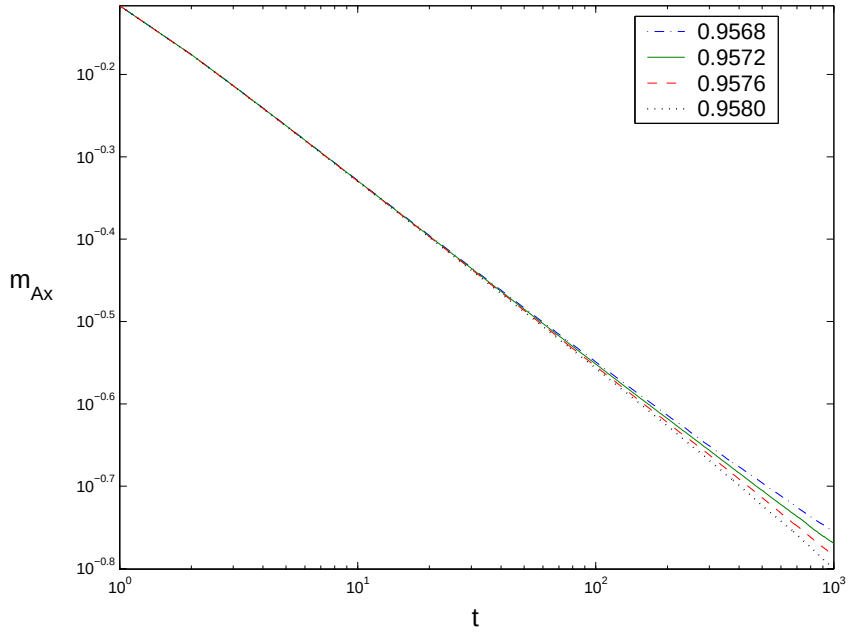

(b)

Figure 6.5: The relaxation of the order parameter m_{Ax} versus t for $r = 0$ (a) on a linear scale and (b) on a log-log scale

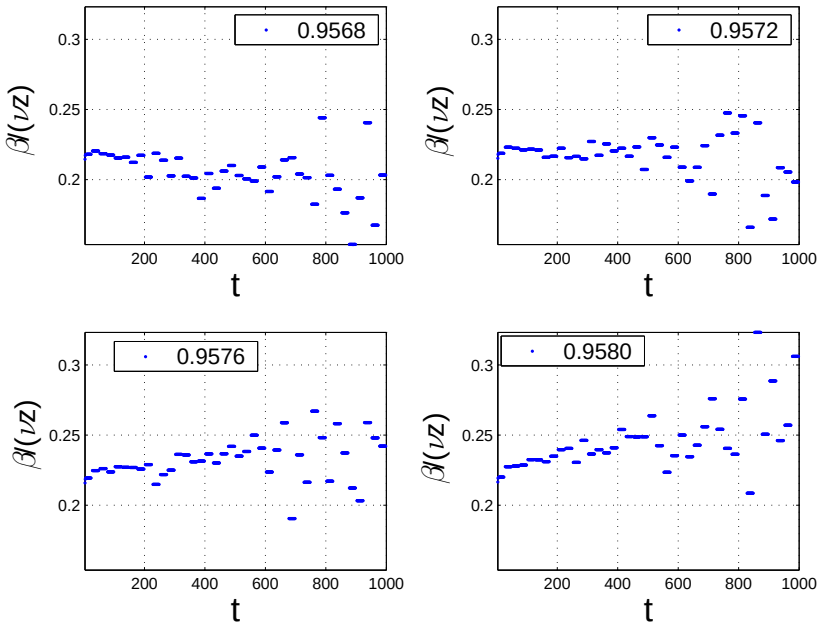

(a)

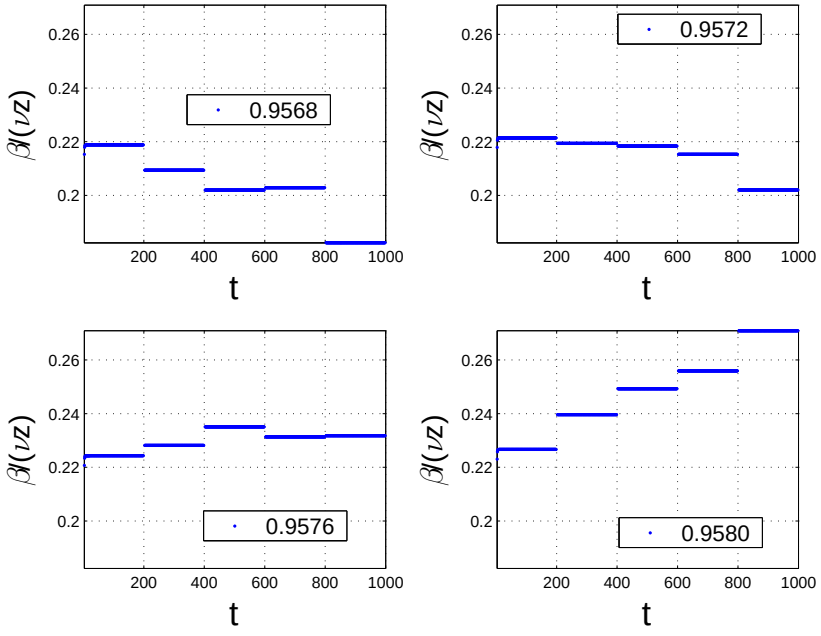

(b)

Figure 6.6: The local exponents vs the successive time intervals at $r = 0$ for (a) $l = 25$ and (b) $l = 200$

a function of t at T_c. After t_{min}, however, the local exponents remain constant up to a t_{max} which is, in the ordered start case, the maximum time we have performed the simulation. This behavior is illustrated in fig. 6.6(a) which shows the local exponents of the successive time intervals with $r = 0$ for $l = 25$. For the temperature $T = 0.9568$, one sees that the exponents decrease after a slight increase at the beginning. This is also the case of $T = 0.9572$, although the decrease is not as clear.

To get a better picture, we should use the same technique for different values of l. In general, smaller values are more suitable to estimate t_{min}, but there is more dispersion associated with them. The larger values of l give us a better understanding of the behavior at larger time. As an example, we have shown the local exponents of the same data for $l = 200$ in fig. 6.6(b) where it is easier to see the gradual decrease of local exponents for $T = 0.9572$. The physical meaning of the decrease is slowing down of the relaxation due to the existence of a non-zero value of the order parameter. As a result, we conclude that $T = 0.9568$ and $T = 0.9572$ are below T_c. However, for the temperatures $T = 0.9580$ and $T = 0.9576$, the local exponents increase. This indicates that the two temperatures are above T_c.

By looking at the figures of this type in which the local exponents are shown as a function of successive time intervals, one comes to two immediate conclusions. First, one can estimate t_{min} which is an important step. This is because a bad estimate of t_{min} would likely lead to inaccurate values of T_c and the critical exponents. The second immediate conclusion is that one is able to estimate the value of T_c. For instance, as we have shown above, one concludes that $0.9576 < T_c < 0.9572$ for $r = 0$. The latter conclusion is possible since one realizes that there exists a temperature in this range for which the local exponents are almost constant after t_{min}.

The scaling behavior for $r = 0$ appears fairly soon at around $t_{min} = 20$. However, this is not the case for all values of r. As an example, we show the relaxation curves of m_{Ax} and the corresponding log-log plot for $r = 20$ in figure 6.7. One sees that linear behavior on the log-log scale plot doesn't emerge at the very beginning. In general,

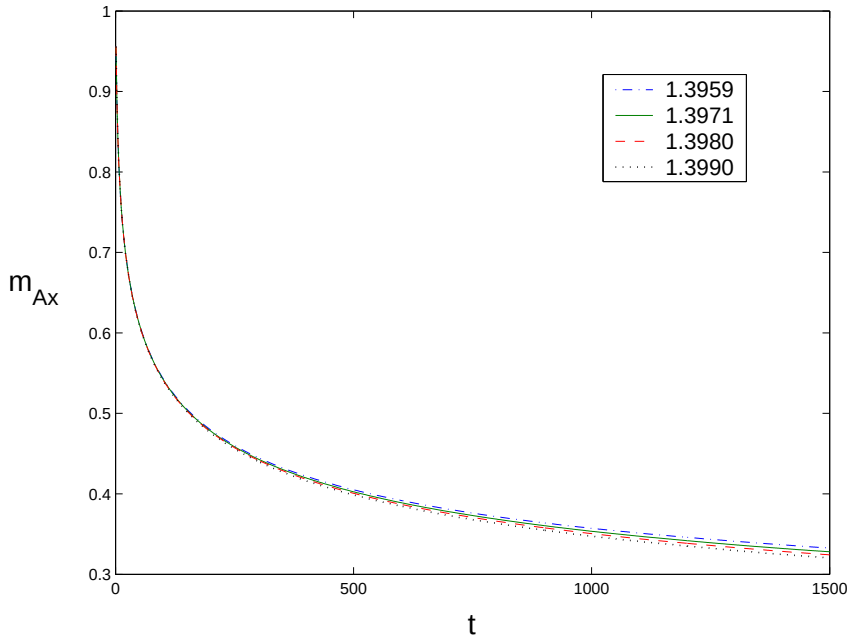

(a)

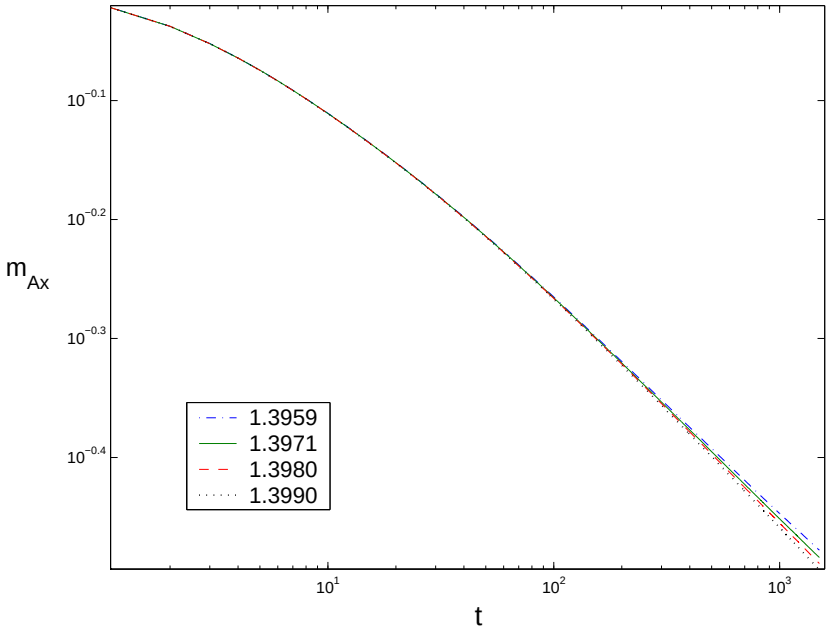

(b)

Figure 6.7: The relaxation of the order parameter m_{Ax} versus t for $r = 20$ (a) on a linear scale and (b) on a log-log scale

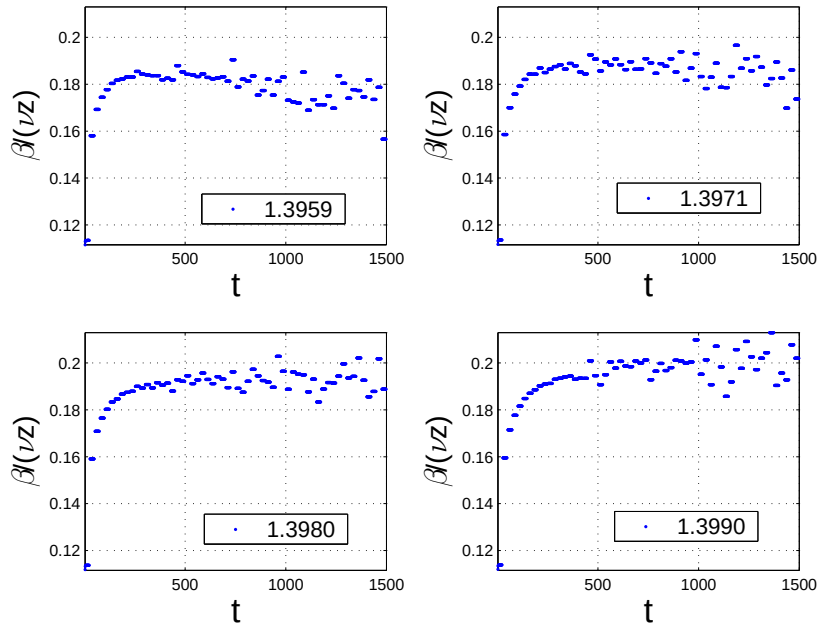

(a)

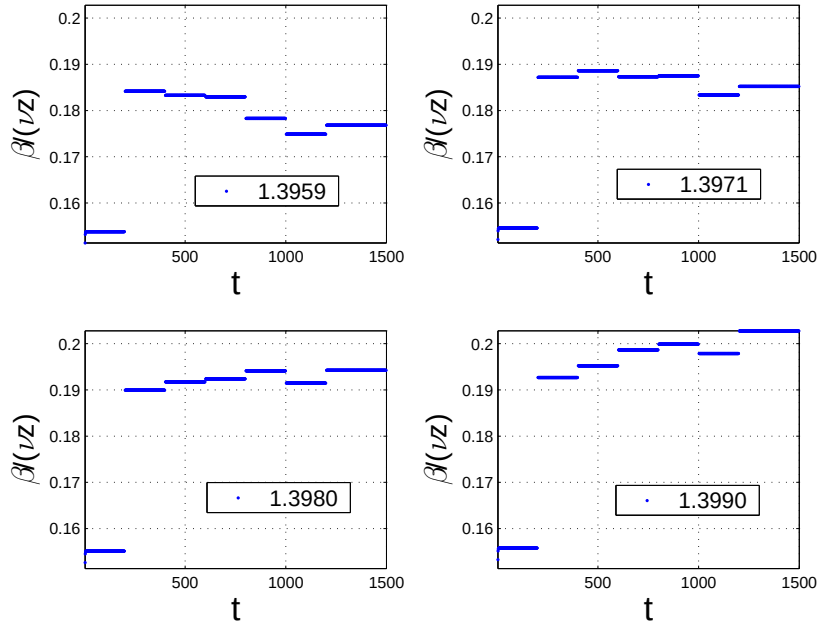

(b)

Figure 6.8: The local exponents vs the successive time intervals at $r = 20$ for (a) $l = 25$ and (b) $l = 200$

t_{min} will grow as r increases. In the $r = 20$ case, for example, the t_{min} is about 300. This can be seen in fig. 6.8 by means a local exponent analysis. Actually this is expected since each spin is under a much stronger local magnetic field, such that the spin system needs more time in order to exhibit a power law behavior. The other effect of a large value of r is the slow relaxation of the order parameter compared to the small values. By comparing the figures 6.5(a) and 6.7(a), we notice that the value of the order parameter for $r = 20$ even at $t = 1500$ is bigger than the one for $r = 0$ at $t = 1000$. This is again due to the large magnitude of local magnetic field on each spin. It is easy to calculate that the local magnetic field on each spin in the GS of the $r = 20$ system is 9 times larger than that for $r = 0$. As $r \to \infty$, due to the single-spin flip nature of the algorithm, the order parameter will not change from its t_0 value and we will have $t_{min} \to \infty$.

So far we have shown the relaxation curves of m_{Ax}. The relaxation behavior of the initially non-zero magnetization components for other sublattices is very similar. As an example, we show the relaxation of m_{By} in fig. 6.9. We can use these other components to calculate T_c and the critical exponents as well. However, the relaxation curves of these components are less accurate than m_{Ax} in the sense that there are more fluctuations associated with them. In general, the components with smaller initial values are less reliable. We justify it in the following way: In order to obtain better results, we average over many equivalent samples. Because the system is a finite size system, there will be small degree of rotation in the direction of the order parameter for each sample. One can see that the components with smaller initial values are more sensitive to these rotations. As a result, there are more fluctuations associated with $m_{Bx}(t)$ than $m_{By}(t)$ and both have more fluctuations around their mean values than m_{Ax}.

We argued that each initially non-zero $m_{\alpha\beta}$ can be used independently to find T_c and the critical exponents. So the final value of T_c and the critical exponents will be an average over the values obtained from these magnetization components. However,

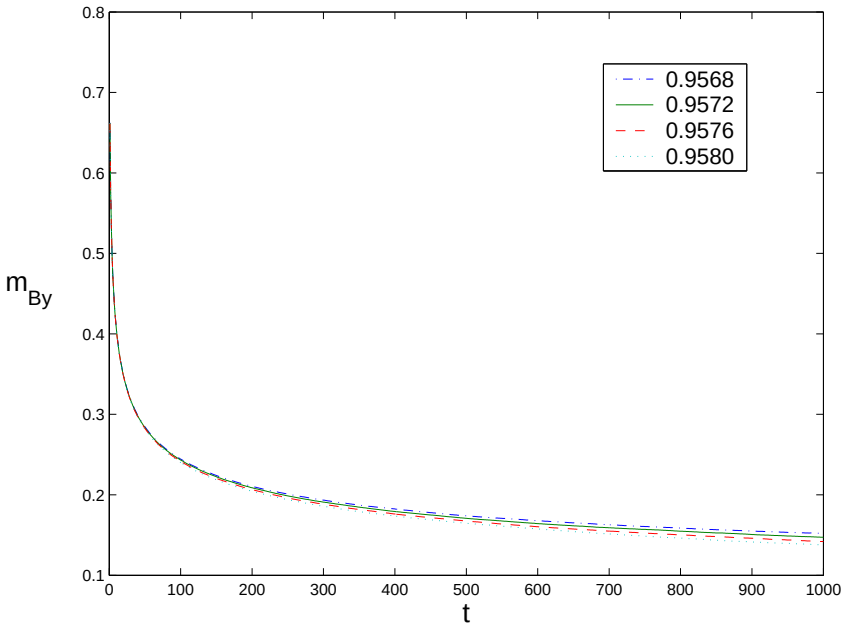

(a)

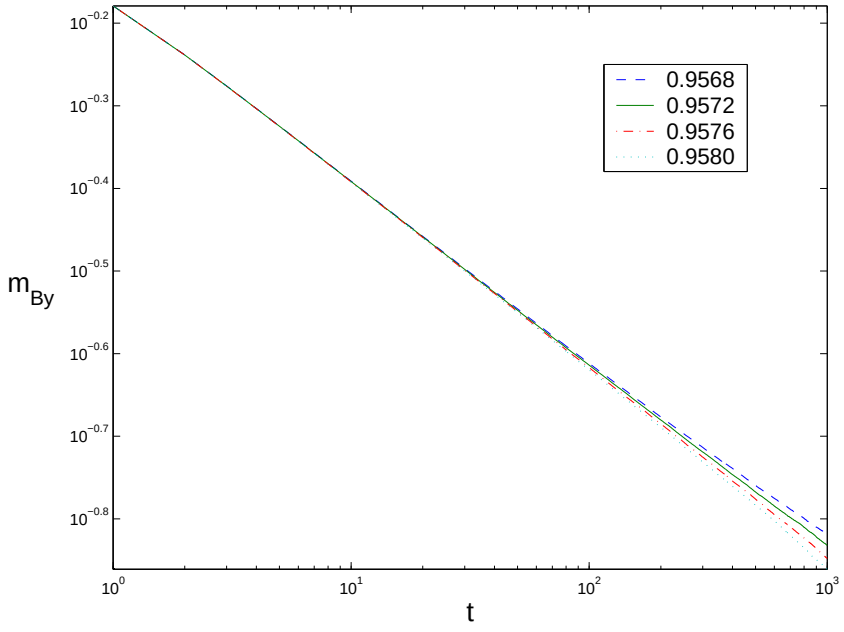

(b)

Figure 6.9: m_{By} versus t for $r = 0$ and four quenched temperatures (a) on a linear scale and (b) on a log-log scale

due to the symmetry of the initial configurations, it is better to use the following quantities

$$m_1 = -(m_{Bx} + m_{Cx})/2 \tag{6.7}$$

$$m_2 = (m_{By} - m_{Cy})/2. \tag{6.8}$$

By doing so, we can, to some degree, remove the effect of the rotations of the order parameter. These two quantities along with the third one m_{Ax} can be used as the order parameters independently.

Since m_{Ax} is more accurate, the result obtained by m_{Ax} should be weighted more than the other components. In other words, we should weight the result of each magnetization component according to its initial value. The reasonable choices of the weighting factors can be the square of their initial values as follows

$$W_{m_{Ax}} = 1$$

$$W_{m_{Bx}} = W_{m_{Cx}} = 0.25 \tag{6.9}$$

$$W_{m_{By}} = W_{m_{Cy}} = 0.75.$$

As a result, the weighting factors of m_1 and m_2 are

$$W_{m_1} = 0.5 \tag{6.10}$$

$$W_{m_2} = 1.5$$

which means that they are simply a sum over the weighting factors of the corresponding magnetization components. We can calculate T_c and the critical exponents associated with each order parameter, and perform a weighted averaging over these values. The error bars can also be easily estimated by calculating the weighted standard deviation of different quantities obtained from these three order parameters.

The errors in our calculations can arise from three different sources. The first type of error is the statistical error of the MC measurement. We can simply average over

many samples to reduce this error. The second source of errors is interpolation. By having a small range of quenched temperatures, we can minimize the magnitude of these errors as well. These two sources give rise to the third type of error which is the error in fitting an straight line to the available data. Since the number of the points to be fitted is of the order of 10^3 points, and the points also show a good linear behavior, the value of this third type of error, which implicitly includes the other two types, does not become large. They are calculated and found to be, in general, less than the standard deviation of the three independent results. As a result, the weighted standard deviation calculation provides a more reasonable estimate of error in the final results.

r	-20	-8	-4	-3	-2	-1	0	1	2	4	8	20
t_{min}	350	300	200	170	100	70	20	40	60	80	110	300
t_{max}	1500	1500	900	1000	1000	1000	1000	1000	1000	1000	1000	1500
q	5000	5000	2500	2500	2500	2500	2500	2500	2500	2500	2500	3000

Table 6.1: The t_{min}, t_{max} for various values of r as well as q, the number of independent measurents we have performed for each quenched temperature

The system size we have used is $L^3 = 90 \times 90 \times 90$. $L = 90$ is large enough in order to neglect finite size effects because at the early stage of relaxation the correlation length is much smaller than the system size. To calculate the quantities of interest, we first determine the appropriate intermediate time interval $[t_{min}, t_{max}]$, and then look for the best power law behavior. In Table 6.1, we have summarized the t_{min}, t_{max} for various values of r as well as q, the number of independent measurents we have performed for each quenched temperature. In fig. 6.10, we show the value of the critical temperature as a function of the constraint parameter r. As discussed

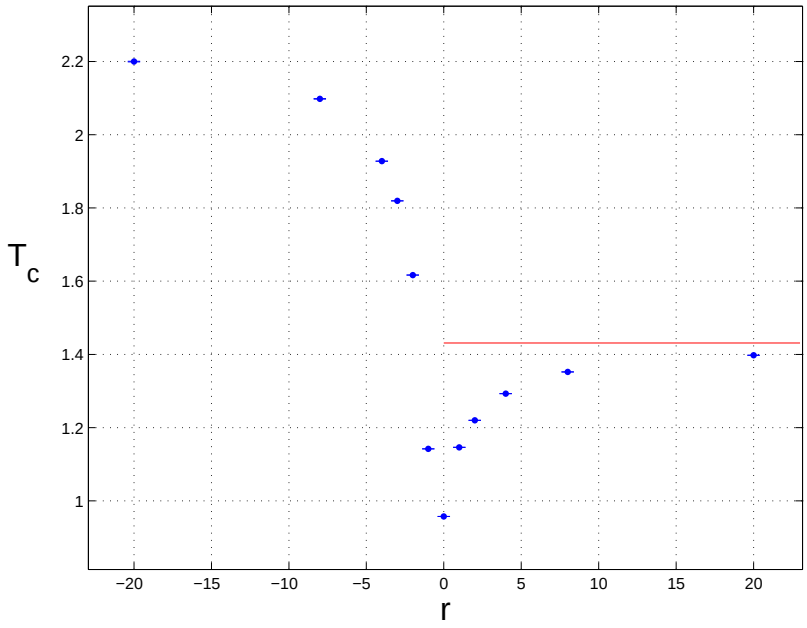

Figure 6.10: The critical temperature T_c vs the constraint parameter r

before, the error bars are the weighted standard deviation of the three independent measurements of T_c for each fixed value of r. They are small and within the thickness of points. Some points and comments on the figure are the following:

- No T_c in the range r (-1,0) is included in the figure. This range covers the kagome lattice and will be discussed later on.

- The rise in T_c, as $|r|$ becomes larger, is expected because the average local magnetic field on spins increases.

- For $r = 0$, the STA model, we have found $T_c = 0.9574(1)$. This value is in good agreement with the previous MC results that are summarized in Table 6.2. This is remarkable since the short-time dynamics approach is quite different from the equilibrium MC simulation which was used in previous studies.

- We expect that T_c approaches to the value of the STAR model as r increases

Ref.	T_c
[52]	0.958(4)
[53]	0.9577(2)
[54]	0.9576(2)

Table 6.2: The critical temperatures of Heisenberg STA system

from zero. The T_c of the STAR model calculated by Loison et al. [51] is 1.43122(12) and is shown as a horizontal line in fig. 6.10. One sees that the value is gradually approached as the constraint becomes stronger. We have not done the calculations for $r > 20$ because our single-spin flip algorithm is not efficient for those large values.

- $r = -\infty$ limit corresponds to the STA model but the "block spins" have twice the interaction constants as the model at $r = 0$ within the layers and the interaction constant between the layers is three times that of the model at $r = 0$. The GS energy of the $r = -\infty$ model is 12/5 times the energy of the STA model at $r = 0$. So the T_c of the system should be close to 12/5 times the value of STA at $r = 0$, that is $\frac{12}{5} \times 0.9574 = 2.2978$. In fig. 6.10, one sees that the value is gradually approached as $|r|$ grows. This is another success for the method that shows consistency with the theoretical predictions.

The slope of the log-log plot of the order parameter versus t at T_c yields the exponent $\beta/\nu z$. The exponents for different values of r are shown in fig. 6.11. The exponent decreases as the constraint becomes stronger. Again this is what we expected because the average local magnetic field on each spin is stronger for larger values of r and therefore the relaxation process is slower. However, one sees that the slope of decrease on the right side is steeper than on the left side. If the decrease had been just due to the magnitude of local magnetic field which is larger for bigger r, then we would have

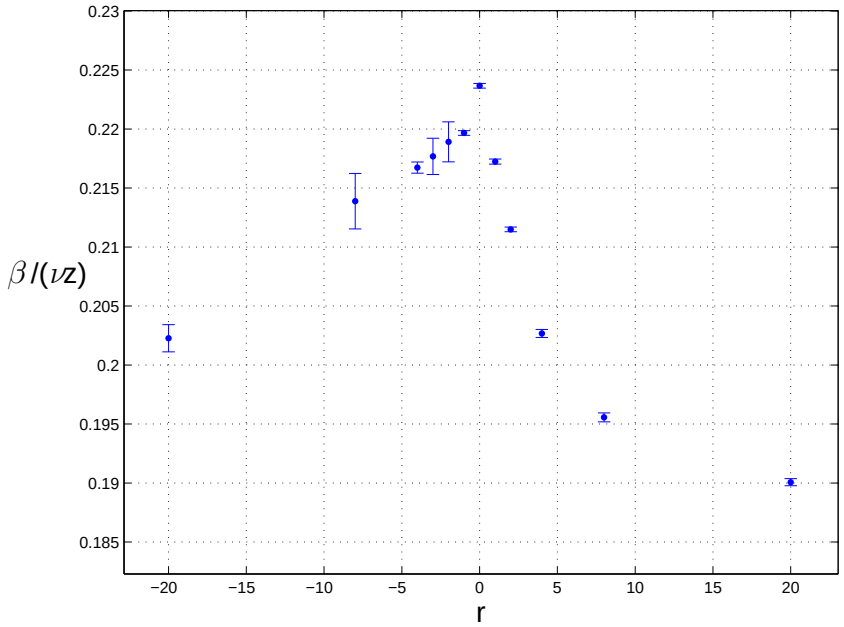

Figure 6.11: The exponent $\beta/\nu z$ versus the constraint parameter r

expected to see a steeper slope for left side. This is because, in negative r region, spins of each plaquette are parallel, so that vector sum of the local magnetic fields due to the neighboring spins of the same plaquette will be larger. As a result, one concludes that qualities of the critical relaxations of these two regions are different. This will be discussed shortly. Similar to the calculation of $\beta/\nu z$, the log-log plot of $\partial_\tau \ln m(t,\tau)|_{\tau=0}$ versus t should be linear with a slope equal to $1/\nu z$. For $r = 0$, this linear behavior of the quantity on a log-log scale is plotted in fig. 6.12. The value of $1/\nu z$ as a function of r is plotted in fig. 6.13. A jump in the value at $r = 0$ to that at $r = 1$ is interesting. According to equation (3.19), this implies that the correlation time for $r = 0$ case is larger than the $r = 1$ case.

Combining equations (5.11) and (5.10) it is easy to see that $\langle m^2\rangle - \langle m\rangle^2$ shows a power law behaviour with the exponent $(d - 2\beta/\nu)/z$. So we can calculate z without using the binder cumulant directly, provided that we have already found the exponent $\beta/\nu z$. The dynamic exponent z is shown as a function of r in fig. 6.14. In general, z

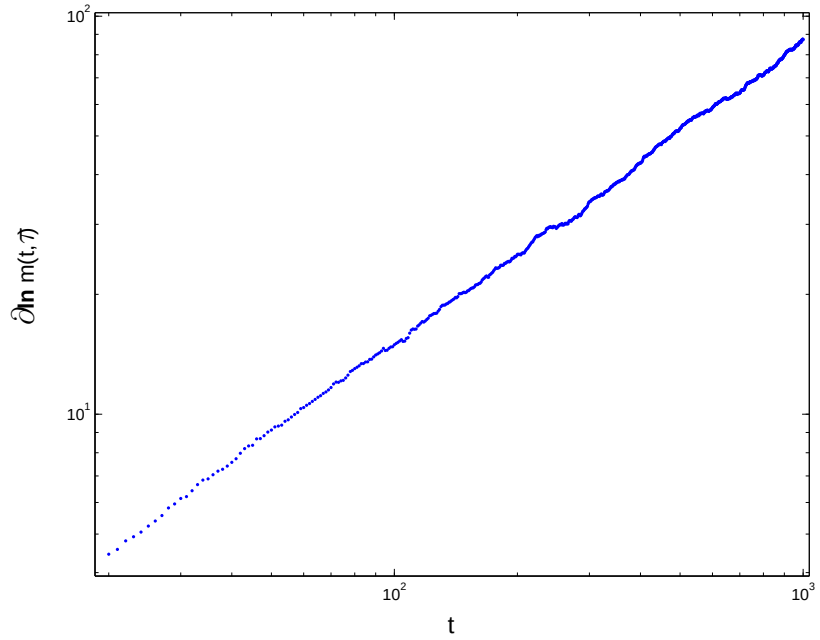

Figure 6.12: $\partial_\tau \ln m(t,\tau)|_{\tau=0}$ versus t on a log-log scale in the intermediate time range $[20, 1000]$

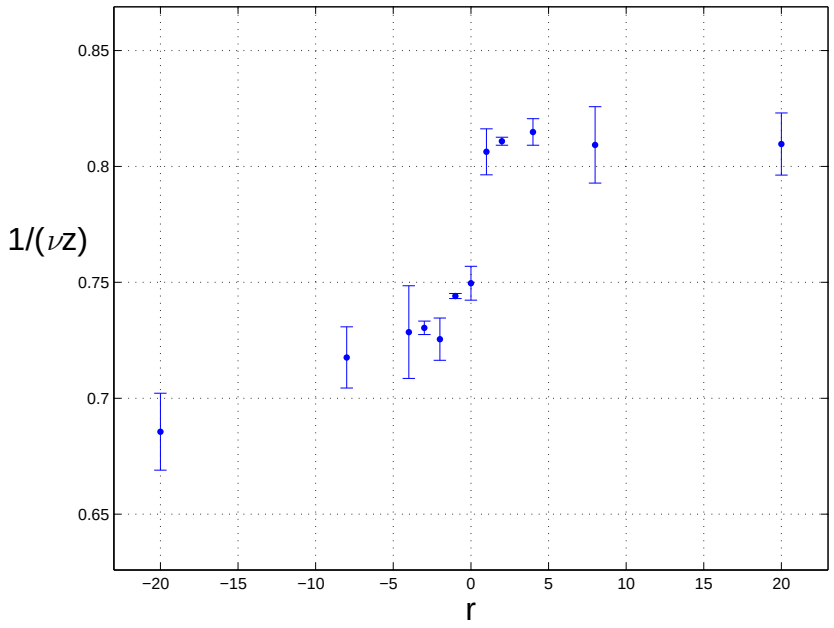

Figure 6.13: The exponent $1/\nu z$ vs the constraint parameter r

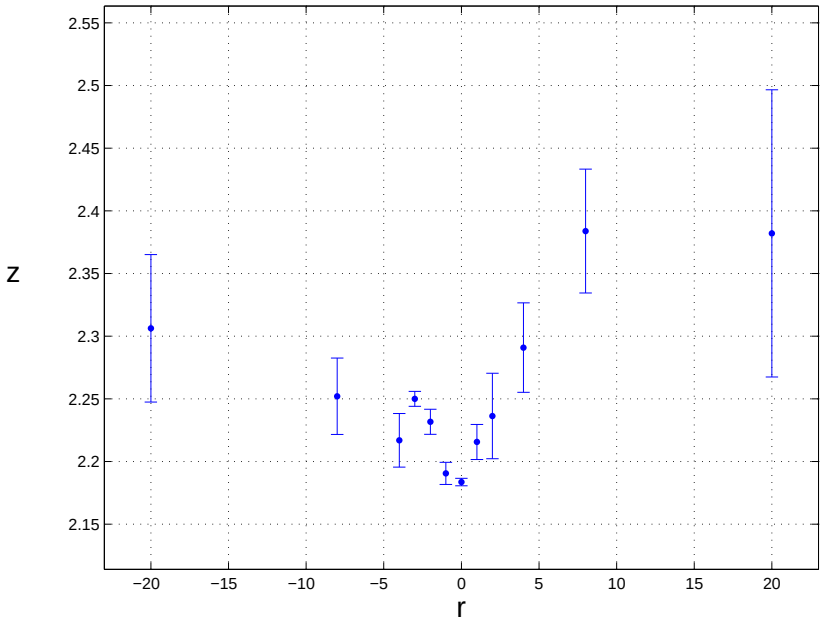

Figure 6.14: The dynamic critical exponent z vs the constraint parameter r

depends on the algorithm as well as the model. The algorithm has not been changed, so the change in z is entirely due to the model. Since z is a measure of how efficient the algorithm is in equilibrium, the increase in z is expected as $|r|$ grows.

So far we have exploited all the scaling relations available for an initial ordered configuration, and calculated the corresponding slopes. Now we are able to find the static exponents β and ν. Figure 6.15 shows the exponent β versus the constraint parameter r. For $r = 0$, the STA model, we have found $\beta = 0.298(3)$ which overlaps with the values obtained in previous studies (see table 4.3). The solid line in fig. 6.15 shows the β value of STAR model calculated by Loison et al. [51]. For positive r, one notices that β decreases as r increases. Similar to case of T_c, β gradually approaches to the value of the STAR model as $r \to \infty$. This is again in agreement with our expectations. For negative r, on the other hand, β is almost unchanged as $|r|$ increases. This fixed value seems to be equal to the value at $r = 0$ which also corresponds to β in the limit $r \to -\infty$. We once again note that the r range $(-1, 0)$

will be discussed later.

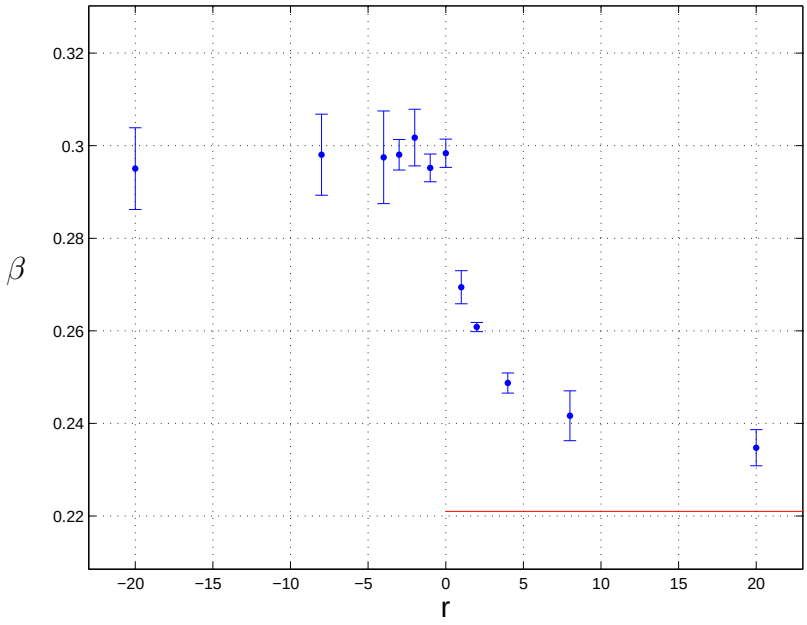

Figure 6.15: The critical exponent β vs the constraint parameter r

In addition, figure 6.16 shows the exponent ν as a function of r with a solid line corresponding to the value of the STAR model. The value at $r = 0$ is 0.611(7) which is rather consistent but about (3-4)% larger than the one obtained by equilibrium MC simulation. This is not surprising if the phase transition is a first order phase transition. One sees that the STAR value is smoothly approached as the constraint parameter is tuned up. Interestingly, the exponent ν versus r exhibits the same behavior as the exponent β. In the negative r region, the exponent ν is not sensitive to changes in the constraint parameter and is within the error bar of the exponent ν at $r = 0$. However, for positive r, ν falls as the r increases.

From the behavior of the exponents β and ν in the positive r region, one concludes that the critical behavior associated with the model changes as the constraint parameter varies. This would have been unexpected if we were sure that the phase transition is a second order one because all we do is to make the interaction bonds

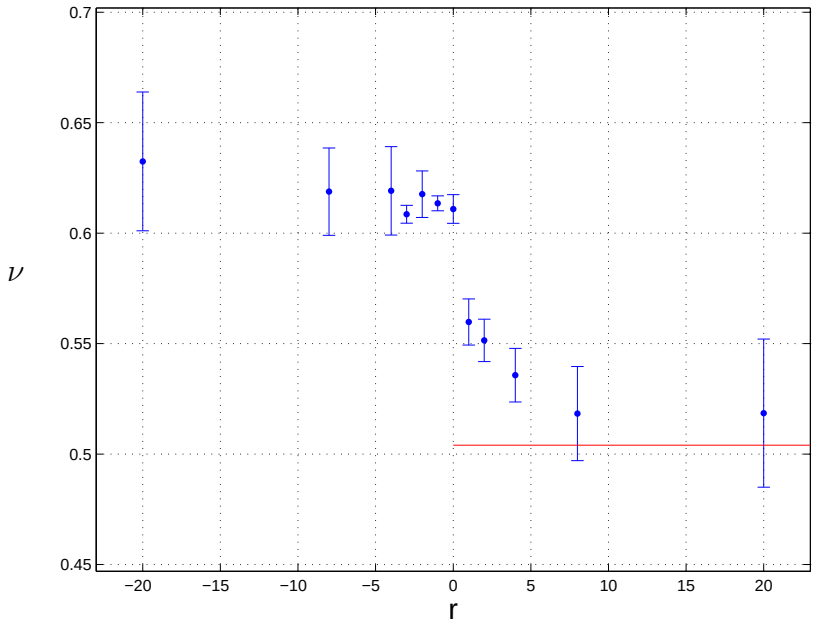

Figure 6.16: The critical exponent ν vs the constraint parameter r

between spins in each plaquette stronger but the symmetry is not changed. In fact, the variation of the critical behavior implies that the nature of the phase transition changes by tuning the constraint parameter. This corresponds to a non-universal behavior that is inconsistent with a second order phase transition. Hence our results suggest a weak first order phase transition.

For negative r, we found that the exponents do not strongly depend on r. This implies that the critical behavior, and therefore the nature of the phase transition, does not change as r varies. In particular, the range of these exponents are within the error bar of the $r = 0$ values which correspond to the values in the $r = -\infty$ limit. This means that the nature of phase transition is the same in the range $[-\infty, -1]$. Suppose we are in the $r = -\infty$ limit where the spins in each plaquette are locked together and point in the same direction. If we unbind the constraint smoothly, the spins of one plaquatte start to fluctuate with respect to each other at a non-zero temperature. These fluctuations are non-critical and do not change the critical behavior. As a

consequence we observe a universal behavior in the negative r range. This is a great success for the model since it reveals both the universal and non-universal behavior of Heisenberg frustrated systems which is already observed in experimental studies.

The variation of r does not change the global symmetry of our model. However, it changes the local symmetry of each spin in a sense that, for each spin, the directions of the two neighbors from the same plaquette becomes more special than the other directions. Our results tell us that the critical behavior associated with these systems does not change as long as the spins of each plaquette are in the same direction and no local chirality exists. However, as the interactions become antiferromagnetic and the local chirality can be defined for each plaquette, the critical behavior becomes dependent on the details of the interactions and the nature of the phase transition changes.

For $d = 3$, the scaling relation (2.18) reduces to the following relation

$$\eta = 2\beta/\nu - 1, \tag{6.11}$$

which enables us to calculate the anomalous dimension η. We have shown η as a function of r in fig. 6.17. For all values of r, the anomalous dimension is negative. Following the argument of Loison et al. [51], this provides further indications that the phase transition is a first order phase transition.

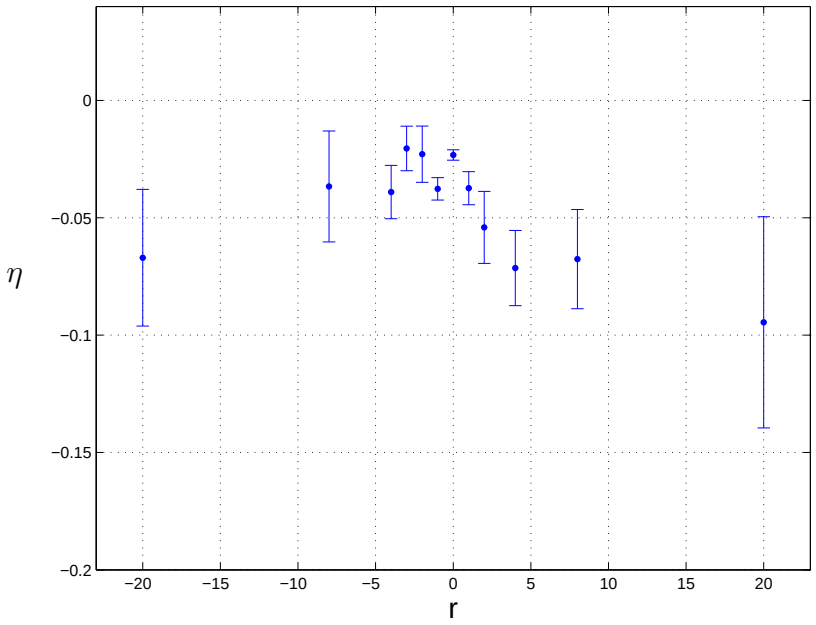

Figure 6.17: The anomalous dimension η vs the constraint parameter r

6.3.2 Disordered configuration start

We already found that the nature of phase transition changes as the constraint parameter varies in the positive r region. In this region, by tuning the parameter, we smoothly suppress the non-critical modes such that the first order behavior will become more apparent. In particular, we found that the anomalous dimension becomes more negative as r increases. This suggests that the phase transition becomes a stronger first order transition. We can investigate this suggestion by means of metastability since, as discussed in chapter 5, one can distinguish a second order phase transition from a first order one by looking for the metastability.

The relaxation curves of an ordered initial state are more accurate and better quality than those of a disordered start. Actually, there is less error associated with the result of an ordered start. In addition, we can obtain all the critical exponents from an ordered configuration start. As a result, we do not need to perform the calculations for a disordered configuration start if we are only interested in the critical exponents. However, in order to estimate metastability, we should calculate the transition temperature associated with a disordered configuration start. This is the motivation to simulate the relaxation process starting from a disordered state.

For a disordered configuration start, the value of the critical temperature, as well as the exponent θ, is dependent on the initial value of the order parameter m_0. The scaling form (5.6), however, is only valid in the limit $m_0 \to 0$, so that the right value of θ and T_c can only be obtained in this limit. Practically, it is difficult to obtain a good relaxation curve of the order parameter for very small values of m_0. One way to avoid performing calculations for very small m_0 is to do the simulation for different values of m_0 which are not too small, and then extrapolate θ and T_c to $m_0 = 0$. In fact, this is what one must do if one is to find θ. However, because we are interested in the value of T_c, not θ, we can use alternative scaling relation such as (5.8) to work with. Instead of m, we follow the time dependence of the quantity

$|m| = \sqrt{m^2}$. It can be found that $|m|$ exhibits a power law behavior at T_c with the exponent $(d - 2\beta/\nu)/2z$. So T_c can be determined by searching for the best power law behaviour of this quantity rather than m.

The order parameter $|m|$ can be defined in the following way:

$$|m| = (|m_A| + |m_B| + |m_C|)/3 \tag{6.12}$$

which means that $|m|$ is the average of the absolute value of the sublattice magnetizations. Although we can use any of the $|m_\alpha|$ quantities as the order parameter independently, $|m|$ provides us with more accurate results. However, like the ordered start case, the results of $|m_\alpha|$ are used to estimate the error bars. By using $|m|$, we are able to select the initial state as a state of complete disorder. Because the system is a finite size system, there will be a very small value of m_0, and we see that $|m|$ grows as t evolves. Figure 6.18(a) shows such a behavior for $r = 0$ and four quenched temperatures. The corresponding log-log plot is also shown in fig. 6.18(b). We also use the same technique as an ordered configuration start to estimate t_{min}. However, one must be more careful when estimating t_{max}. Despite the initial increase at $T = T_c$, $|m|$ will eventually start to decrease as the system moves to long-time regime. This is because the equilibrium value of m is zero at T_c. In other words, $|m|$ does not keep increasing at the same rate once it is reasonably large. To deal with this effect, we have set a cut-off value $|m| \approx 0.8$ if applicable. It means that the t_{max} will be chosen to be the approximate time at which $|m| = 0.8$ provided that $|m|$ reaches the cut-off value for the expected T_c. By doing so, we don't look at the behavior of the order parameter after it becomes large.

Table 6.3 summarizes t_{min}, t_{max} and q, the number of MC equivalent samples we average over for each quenched temperature. By looking for the best fitted straight line to $\log m$ vs $\log t$, we can find T_c and the exponent $(d - 2\beta/\nu)/2z$. In fig. 6.19, we have shown the value of the exponent $(d-2\beta/\nu)/z$ as a function of r measured by both the initial configuration runs. If the initial configuration is ordered, the exponent

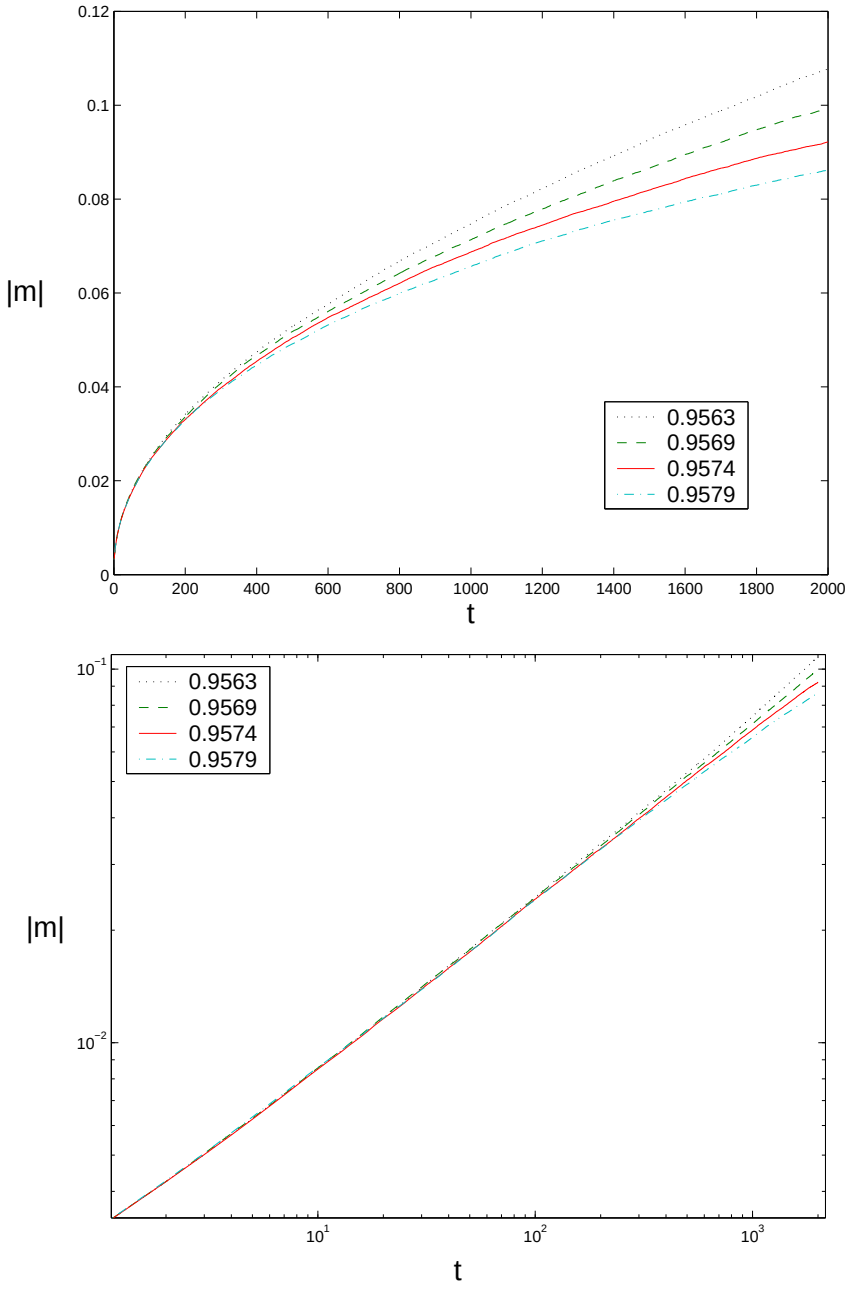

Figure 6.18: The absolute value of the order parameter versus t for four quenched temperatures and $r = 0$ of an disordered configuration start (a) on a linear scale and (b) on a log-log scale

r	0	1	2	4	8
t_{min}	40	75	100	120	125
t_{max}	1400	1800	2000	2000	2000
q	5000	5000	5000	5000	10000

Table 6.3: t_{min}, t_{max} and q for various values of r

is the one associated with the quantity $m^{(2)} - m^2$. For a disordered start, however, it is two times the exponent associated with power law behavior of $|m|$. Both initial configuration runs are in rather good agreement on the exponent.

In order to measure the amount of metastability, we define the following parameter

$$\Delta T_c/T_c = 2(T_{c2} - T_{c1})/(T_{c2} + T_{c1}) \tag{6.13}$$

where $T_{c1}$and T_{c2} are the critical temperatures found by disordered and ordered configuration starts respectively. Figure 6.20 shows the metastability parameter as a function of r. For all the values, the parameter is positive which implies the existence of metastability. As we expected, there is not a considerable amount of metastability involved in the $r = 0$ case. However, one sees that the parameter grows as r increases. This confirms the suggestion that the phase transition becomes stronger first order for larger value of r. The metastability parameter associated with $r = 8$ is larger than the one for $r = 0$ but still in the order of 10^{-3} which is small. This shows that the phase transition remains a weak first order transition even at $r = 8$. In fact, from the beginning we did not expect large metastability involved since good pseudo-scaling behavior was already seen for both STA and STAR models which means that the phase transition is not strong enough to exhibit large metastability.

Now we may feel free to use the word "pseudo-scaling" behavior instead of "scaling" behavior. This is because the phase transition is found to be first order and the "scaling" behavior associated with the system only fakes a true scaling behavior

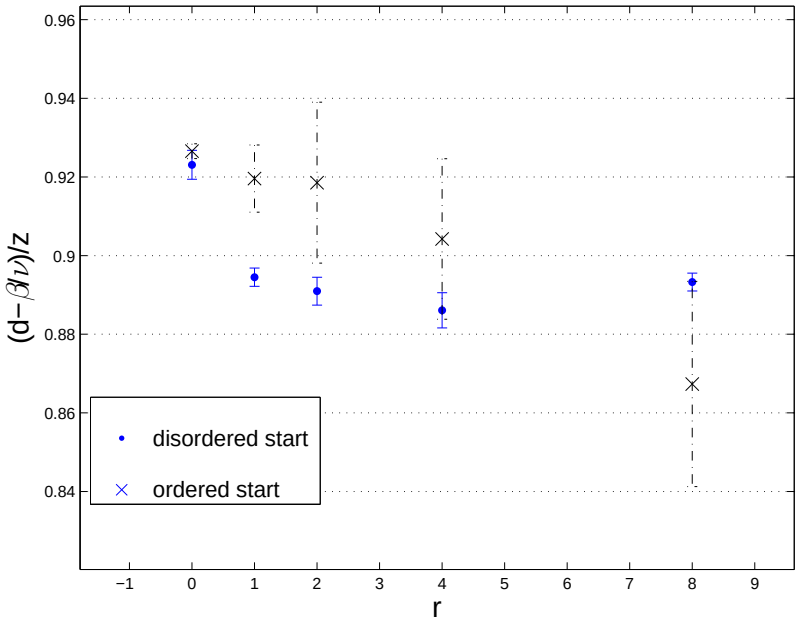

Figure 6.19: The exponent $(d-2\beta/\nu)/z$ versus r. For a disordered start, the exponent is the one associated with the power law behavior of $|m|$ which is compared to the one already calculated for the ordered start

which is only valid for a second order phase transition. The final point is that, in the $[0, \infty]$ range, the STA model corresponds to the weakest first order behavior. One may ask why this is the case. An immediate answer is that because the STA model has the highest local symmetry. In fact, in previous MC studies [53], two types of order parameter, magnetic and chiral order parameter, were considered to find T_c. This has led to two measurements of the critical temperature: magnetic and chiral transition temperature. These two were found to be the same within the error bars for the STA model. However, the crucial question arises whether we can separate these two transition temperatures by destroying the local symmetry of the STA model, that is by increasing the constraint parameter from zero. In our calculations, we only measured the magnetic type of the order parameter, so further research work must be done in order to investigate this question.

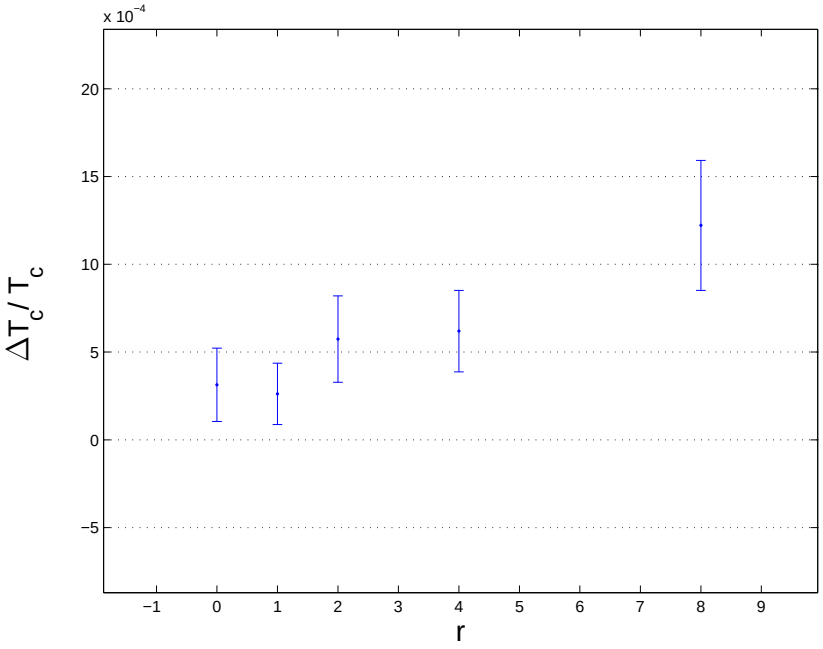

Figure 6.20: The metastability parameter as a function of r in the positive r region.

6.4 Near $r = -0.5$

In this section, we examine the critical behavior of our model for the constraint parameters near $r = -0.5$. We argued that $r = -0.5$ corresponds to the stacked Kagome antiferromagnet. The GS of the Kagome lattice in $d = 2$ is highly degenerate. In fact, the infinite number of GS available for the system suggests that there is no order even at zero temperature [64]. However, low-temperature expansions show that coplanar short-range order occurs as $T \to 0$ with no indication of a finite temperature phase transition [65]. This is supported by MC simulation analysis [65, 66, 67]. There are two well-known (possible) GS that are often used to consider possible long-range order in the system. Figure 6.21 shows these two GS, the so-called $\sqrt{3} \times \sqrt{3}$ state and $q = 0$ state.

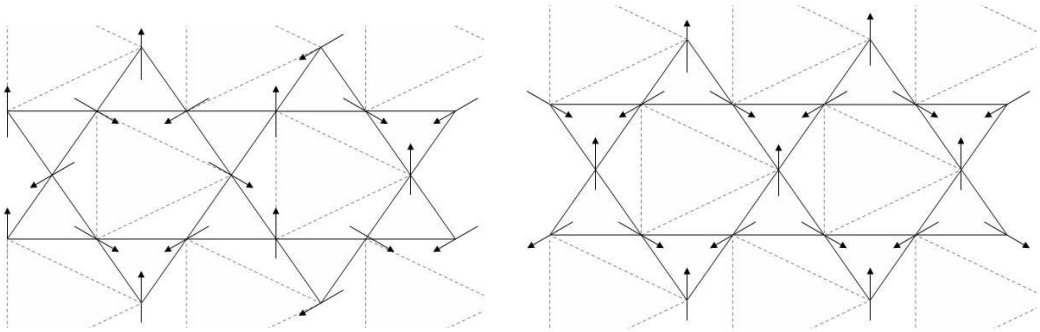

(a) (b)

Figure 6.21: Two possible ground states of the Kagome antiferromagnetic lattice (a) $\sqrt{3} \times \sqrt{3}$ state (b) $q = 0$ state

In $d = 3$, we have an antiferromagnet on the stacked Kagome lattice. We are not aware of any study on this system so far, so that we don't know if there is a phase transition at finite temperature. However, the existence of a finite temperature phase transition is not unexpected because the entropy is not extensive in the GS. One can argue that since no frustration arises by the interlayer coupling, the GS within each

layer remains highly degenerate. As a result, there is no long-range order in each layer, and the spin configurations in all layers are the same [63]. As in $d = 2$, the $\sqrt{3} \times \sqrt{3}$ and $q = 0$ states can be used as the possible GS of the stacked Kagome antiferromagnet. It should be remarked that these two GS are exactly identical to the degenerate GS of our generalized model at $r = -0.5$. The $\sqrt{3} \times \sqrt{3}$ state corresponds to the GS of $r < -0.5$ and $q = 0$ state corresponds to that of $r > -0.5$.

r	-0.6	-0.55	-0.45	-0.4
t_{min}	180	300	250	180
t_{max}	1000	1000	1100	1000
q	2000	2000	2000	2000

Table 6.4: t_{min}, t_{max} and q for various values of r near -0.5

We have only performed the simulations from an ordered initial configuration. The method of obtaining the result and error bars are similar to section 6.3. Table 6.4 summarizes t_{min}, t_{max} and q, the number of MC equivalent samples we average over for each quenched temperature. One notices that t_{min} for the values of r close to -0.5 is larger than the ones for $r = -1$ and $r = 0$. This should be compared to the behavior of t_{min} in the positive r region, where t_{min} increases as r becomes larger. In the last section, we argued that this is because of the single-spin flip nature of our algorithm. However, near $r = -0.5$, the algorithm are just fine. The increase in t_{min} is due to the highly degenerate structure of the GS at $r = -0.5$. In fact, as we get closer to $r = -0.5$, the scaling behavior emerges at later times.

Figure 6.22 shows the T_c as a function of r for the r values of Table 6.4. The error bars are within the thickness of the points. One sees that T_c decreases as the constraint parameter approaches $r = -0.5$. This is predictable since the average local magnetic field on each spin gets weaker. As shown in the figure, one also expects the slope of decrease becomes steeper for r values closer to -0.5. This tells us that if

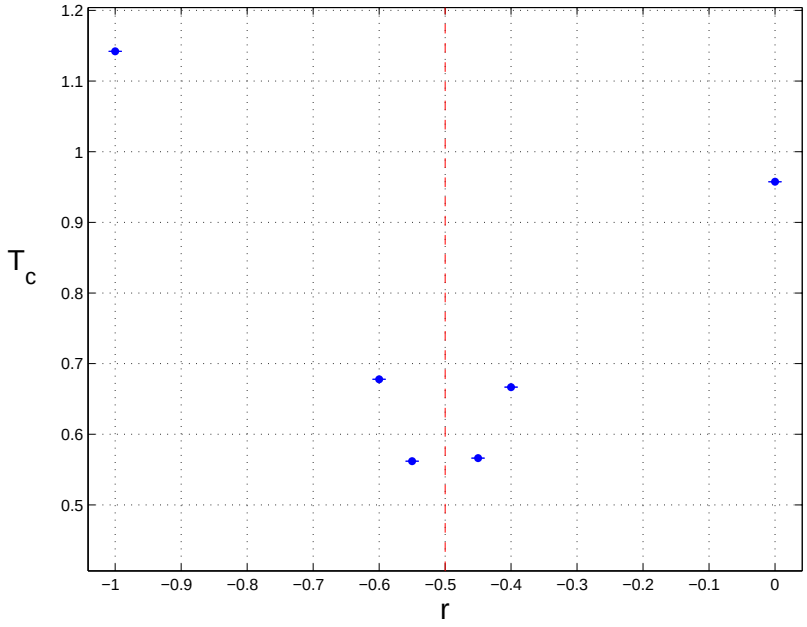

Figure 6.22: T_c versus r near $r = -0.5$

there is a transition at a finite temperature for -0.5, the temperature has to be small.

Figure 6.23 shows the exponent β versus r near $r = -0.5$. The exponent decreases as r approaches -0.5. The reason is the slow relaxation of the order parameter due to the appearance of degeneracy. One sees that the decrease on the right side is faster than on the left side. This is rather justified because the energy of perturbations from the Kagome lattice on the left side is twice as that of the right side. In other words, for a fixed value $|r - 0.5|$, the $\sqrt{3} \times \sqrt{3}$ state, where spins are parallel in each plaquette, is more perturbed than the $q = 0$ state.

However, on both sides, β decreases sharper as r becomes closer to -0.5. So one might expect the critical exponent to approach zero as $r \to -0.5$. To test this expectation, we have also run the simulation for $r = -0.505$ and $r = -0.49$. These values are very close to the kagome limit such that the system is practically degenerate at a finite temperature. This is because the energy barrier between the two degenerate configuration can be easily overcome by thermal fluctuations. For $r = -0.49$, we see

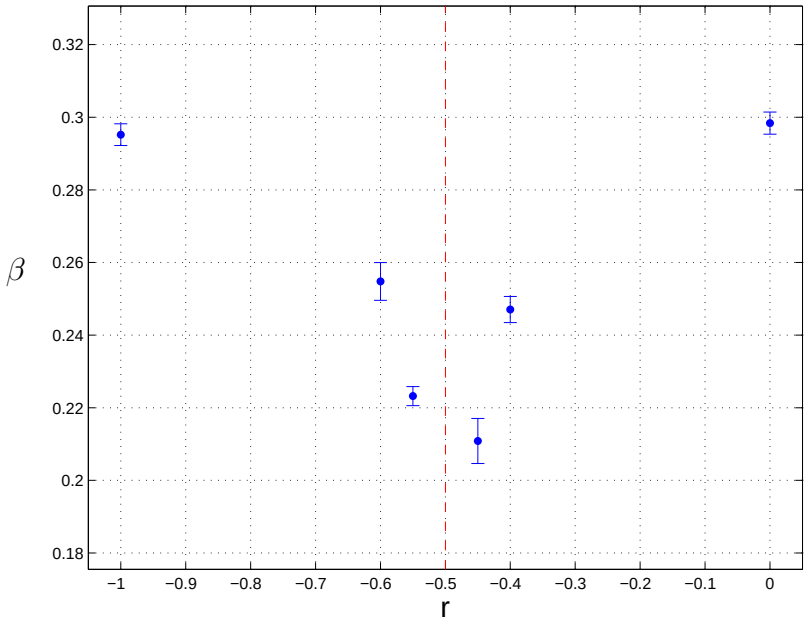

Figure 6.23: The exponent β versus r near $r = -0.5$

that the order parameter relaxes very slowly as shown in fig. 6.24(a) for four quenched temperatures. In fact, we have found that the relaxation can be described by

$$m \sim 1/\log t. \tag{6.14}$$

To demonstrate this, in fig. 6.24(b), we have shown that $1/m_{Ax}$ versus t on a semilog scale exhibits a linear behavior. For a finite value of $\beta/\nu z$, we know $1/m \sim t^{\beta/\nu z}$, but here according to (6.14), we have $1/m \sim \log t$. This implies that $\beta/\nu z = 0$ since such a "logarithmic" behavior is a special case of the power law in the limit that the exponent goes to zero. $\beta/\nu z = 0$ itself means that $\beta = 0$. On the other hand, $\beta = 0$ indicates that the magnetization changes discontinuously from zero to a finite value at the transition temperature [68]. As a result, the transition (if any) is first order.

However, for $r = -.0505$, the situation is different. Figure 6.25 shows the relaxation of m_{Ax} as a function of time for a few quenched temperatures at $r = -0.505$. We have not been able to find a scaling behavior of power law of inverse-logarithmic

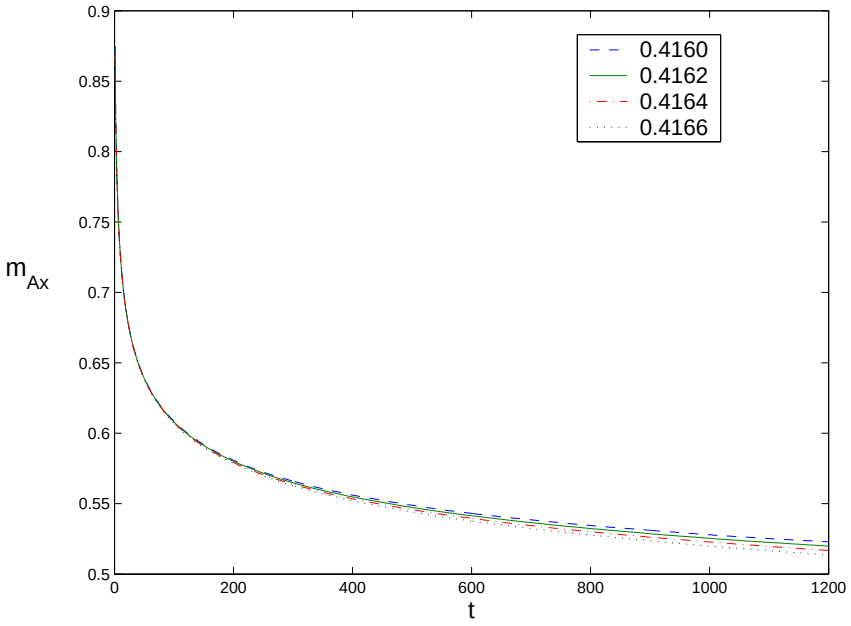

(a)

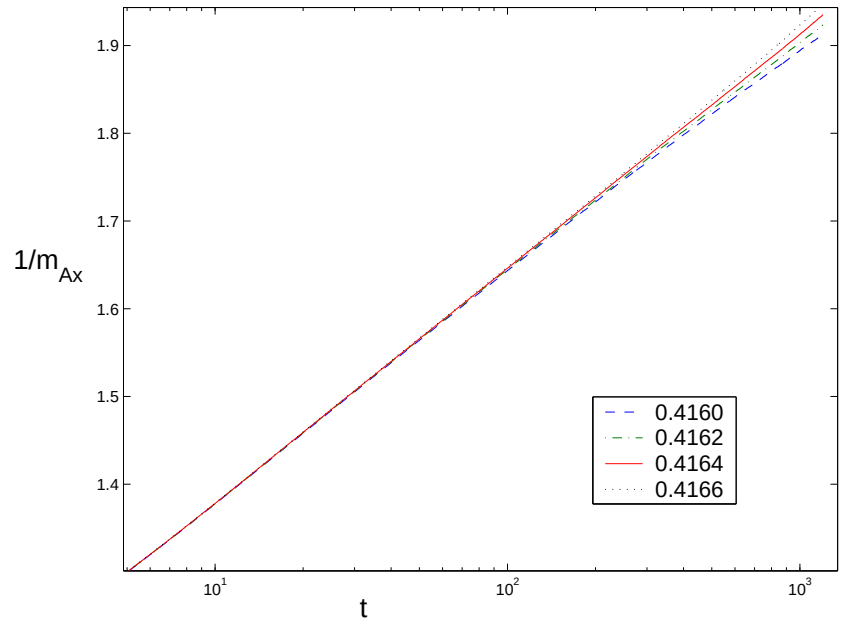

(b)

Figure 6.24: For $r = -0.49$ (a) m_{Ax} versus t for $r = -0.49$ (b) $1/m_{Ax}$ versus t on a semilog scale

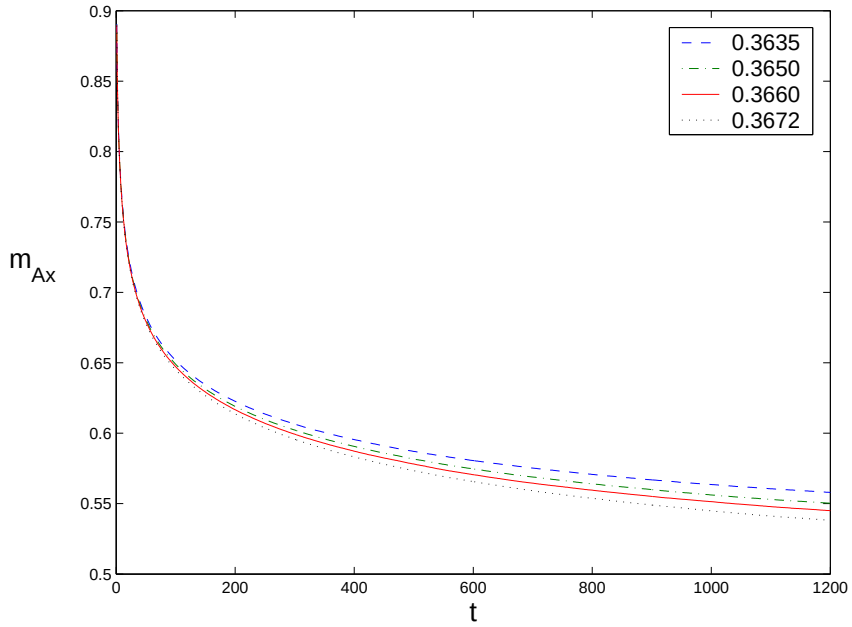

Figure 6.25: The m_{Ax} versus t for $r = -0.505$

type for this value of r. This can be due to a few reasons. First of all, because we expect the relaxation to be slow, the scaling behavior might emerge so late that it can not be detected in our finite time interval. Second of all, this can be due to the first order nature of the phase transition, since we know that there is no scaling behavior for a (strong enough) first order phase transition. Now, the interesting question arises why this same argument is not applicable to $r = -0.49$. The answer is easy. The differences in the scaling behavior is because the nature of phase transition is different on either sides of $r = -0.5$. This implies that the two GS do not behave in the same way at a finite temperature, although they have the same energy at $T = 0$. The differences in these two GS have been already found in $d = 2$ [65, 67]. They can be discussed based on the so-called weathervane defects. As shown in fig. 6.21(a), for $\sqrt{3} \times \sqrt{3}$ state, all the neighboring spins for any hexagon are in the same direction. As a result, the spins in a hexagon can rotate about a common axis with no cost of energy. This shows that the spins of the $\sqrt{3} \times \sqrt{3}$ can be locally perturbed. However,

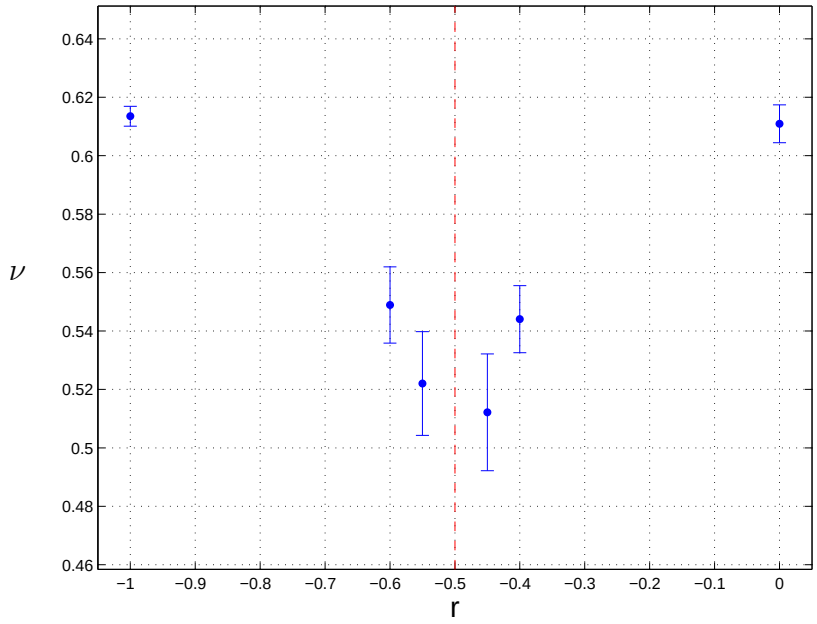

Figure 6.26: The critical exponent ν versus r near $r = -0.5$

for $q = 0$, the zero energy excitations will introduce line defects which span the whole system. MC simulations in $d = 2$ have shown that the $\sqrt{3} \times \sqrt{3}$ structure is thermally more favorable than $q = 0$ at low temperature. In fact, the same differences can be discussed for $d = 3$ which lead to different pseudo-critical behavior on both sides of $r = -0.5$.

Figure 6.26 shows the critical exponent ν versus r and it also decreases as r approaches -0.5. In addition, we have shown the critical exponent η as a function of r. For $r = -0.45$ and $r = -.55$, it is even more negative than the value of the STAR model. This can be an indication that the phase transition is even stronger first order in the vicinity of $r = -0.5$. In fact, $\beta = 0$ implies that $\eta = -1$. According to equation (2.10), this means that the correlation function is independent of distance at T_c. Therefore, the correlation function has to be constant for all distances. This can imply that there is no long-range ordering in the system.

One notices that the critical behavior from $r = 0$ to $r \approx -0.42$ resembles the

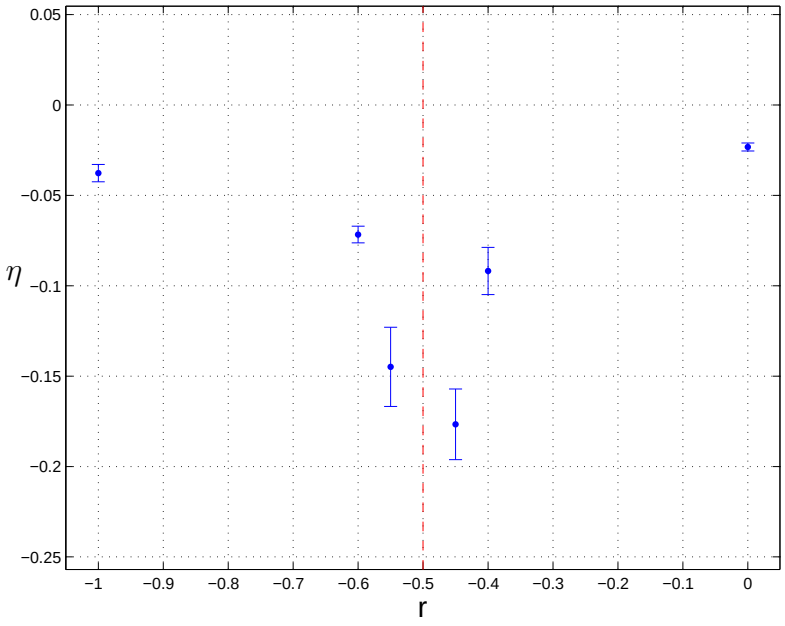

Figure 6.27: The critical exponent η versus r near $r = -0.5$

critical behavior of the model in positive r region in which the critical exponents decrease as $r \to \infty$. The idea was first to suppress the non-critical modes in order to investigate the critical behavior more efficiently. However, by tuning the constraint parameter smoothly from zero to negative values, we actually make the non-critical modes more apparent, such that we do not expect the same type of change in the critical behavior. The question is what this is going to tell us. As discussed before, the local symmetry of each spin changes as r increases from zero. In a same way, we change the local symmetry by switching the constraint parameter to negative r. The critical behavior changes because the local symmetries change. This type of critical behavior which is dependent on local symmetries is not universal and results in a first order phase transition.

6.5 the STAR model

We have performed the simulation for a broad range of r. It is also appropriate to find T_c and the critical exponents of the $r = \infty$ limit which corresponds to the STAR model. In particular, we are interested in investigating the amount of metastability involved in this limit. However, our algorithm is not effective for large values of r, so that we need a plaquette flip algorithm to obtain reliable results rather than a single-spin flip one. It is complicated or maybe impossible to apply a heat-bath algorithm to update the whole plaquette simultaneously. So a Metropolis algorithm which has a straightforward implementation can be used to do so.

In the STAR model, only two of the spins in each plaquette are independent. So to specify each plaquette, we only need two spins (S_1, S_2). We shall refer to these two spins by spin pairs. Each spin pair is determined by three independent angles. Two of these angles establish the direction of the first spin. In the Metropolis algorithm, this direction is chosen at random. The third angle is required to determine the norm vector to the spin pair surface. The latter angle is also chosen at random. We then calculate the interaction energy of the new spin pair with its neighboring spin pairs. To update the spin pair, this energy should be compared with the older interaction energy of the spin pair.

The system size of each sample in the simulation is $54 \times 54 \times 90$ spins pairs. This means that each layer has 54×54 spin pairs. Since each spin pair stands for a plaquette of three spins, 54×54 spin pairs resemble 90×90 single spins which makes the system size equivalent to that of previous simulations.

6.5.1 Ordered Configuration Start

The GS is established for each spin pair as follows

$$\vec{S}_1 = \hat{i}$$

$$\vec{S}_2 = (-\hat{i} + \sqrt{3}\hat{j})/2. \tag{6.15}$$

So the relaxation can be seen for m_{1x}, m_{2x} and m_{2y}. The order parameters can be chosen to be m_{1x} and $\sqrt{(m_{2x})^2 + (m_{2y})^2}$. It should be noted that $m_{i\alpha}$ is the final value of the order parameter after averaging over all samples. As a result, $\sqrt{(m_{2x})^2 + (m_{2y})^2}$ is different from $\sqrt{(|m_{2x}|)^2 + (|m_{2y}|)^2}$.We have carried out the simulation up to 2500 (mcs) for 3500 sample clusters.

The relaxation of the order parameter m_{1x} for four quenched temperatures is shown in fig. 6.28. Figure 6.28(b), the log-log plot of the same data, indicates that the power law behavior of the order parameter emerges very late. We can understand the situation by a local exponent analysis. The local exponents versus the successive time intervals with $l = 75$ for the quenched temperatures are shown in fig. 6.29. One sees that the local exponents appear to remain constant after about 850-900 (mcs). This means that t_{min} is large compared to those of previous studies in this chapter. One reason can be the use of Metropolis algorithm. However, this can also be an indication of a first order phase transition. Remember that we already expected the phase transition to be a stronger first order transition with respect to the STA model. For a first order transition, the correlation time does not become large, so the scaling behavior will not emerge. Notwithstanding, for a weak first order transition, the scaling behavior will emerge but usually late depending on how weak first order the transition is.

In order to have a better estimation of the error bars, we have also performed the calculations for slightly different quenched temperatures. Each of the two order parameters of these two simulations can be used independently to calculate T_c and the critical exponents. The error bars again will be the standard deviation of these four equivalent measurements.

We found the critical temperature to be $T_{c1} = 1.4326(2)$. This value should be compared to $T_c = 1.43122(12)$ which is found by equilibrium MC simulation [51]. Our T_{c1} seems slightly larger than the previous MC result. Let us comment on the difference once we find the T_c associated with a disordered start. The dynamic critical

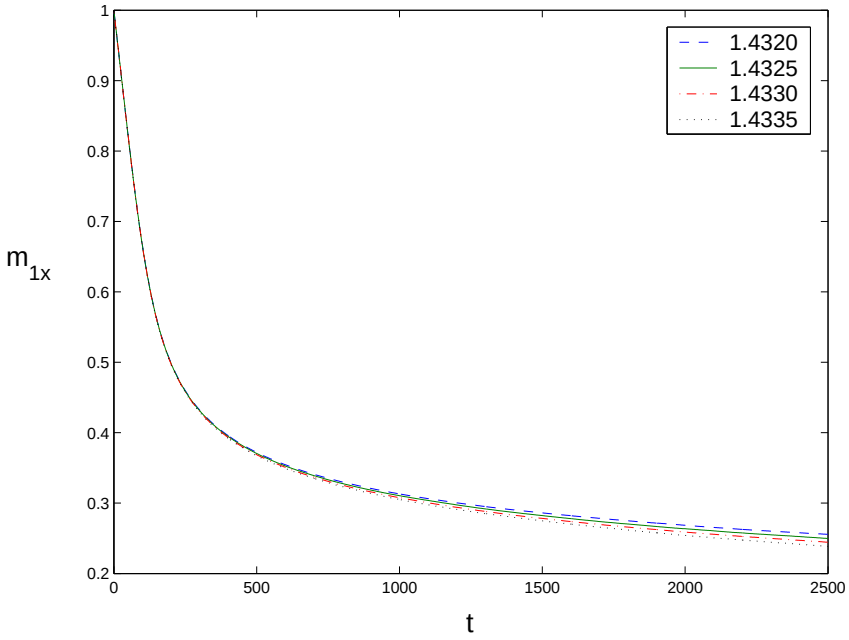

(a)

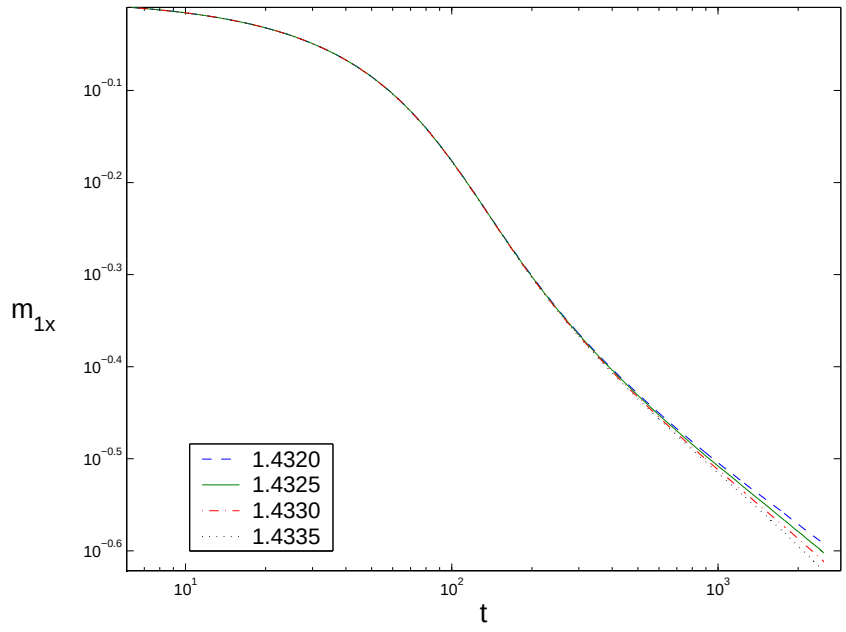

(b)

Figure 6.28: The order parameter versus t for four temperatures (a) on a linear scale and (b) on a log-log scale

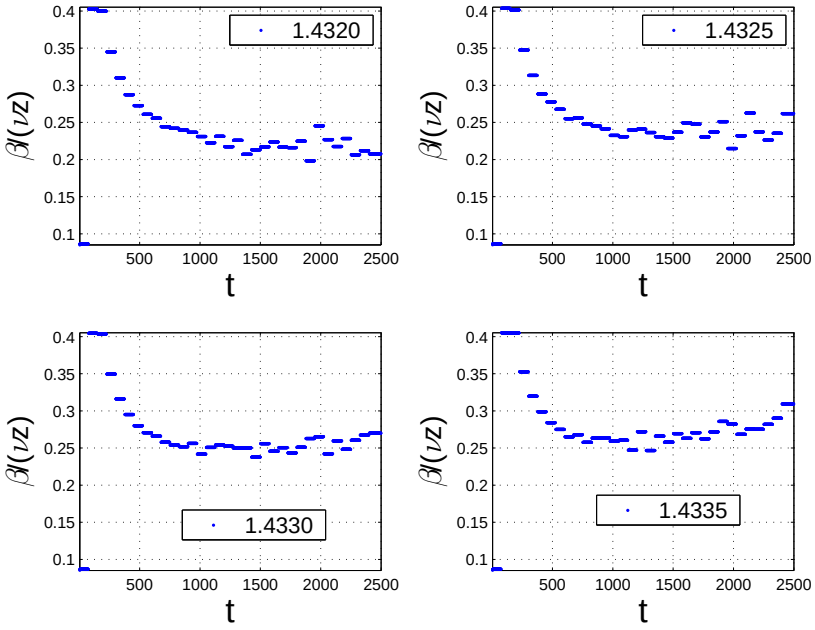

Figure 6.29: The local exponents vs the successive time intervals for $l = 75$

exponent is also obtained $z = 1.877(35)$. The static critical exponents are summarized in Table 6.5 where they are compared to those of previous study. The exponents are in good agreement which is remarkable since the scaling behavior has emerged quite late. The anomalous dimension η obtained to be more negative than those of finite values of r. This can be an indication of a stronger first order phase transition.

6.5.2 Disordered Configuration Start

For a disordered configuration start, we have initialized the system in a state of complete disorder. We have performed the simulation up to 4500 (mcs) for 6000 independent samples. The order parameter is defined as follows

$$|m| = (|m_1| + |m_2|)/2 \tag{6.16}$$

where $|m_1|$ and $|m_2|$ are the average over the magnitude of sublattice magnetization of various samples. Figure 6.30 shows $|m|$ versus t on a linear and log-log scale. To

Exponent	β	ν	η
Our value	0.230(4)	0.512(14)	-0.102(24)
ref. [51]	0.221(9)	0.504(10)	-0.131(13)

Table 6.5: The critical exponents of STAR model, our values compared to the previous study of Loison et al.

find T_c, we have looked at the intermediate time interval [100 : 4500] to search for the best power law behavior. One notices that $t = 4500$, the maximum time we have performed the simulation, is set as the value for t_{max}. This value is not too large because the order parameter has not reached the cut-off value we already defined in section 6.3. The critical temperature is found

$$T_{c2} = 1.4298(2)$$

which smaller than T_{c1} of the ordered start. The metastability parameter is

$$2(T_{c2} - T_{c1})/(T_{c2} + T_{c1}) = 0.0020(3)$$

which implies that considerable amount of metastability is involved. The main point is that the critical temperature calculated by equilibrium MC simulation is in the metastable temperature range $[T_{c2}, T_{c1}]$. In fact, the quantity $(T_{c2}+T_{c1})/2 = 1.4312(2)$ is in excellent agreement with that T_c. This indicates that it is difficult or maybe impossible to find the metastability in a (relatively) weak first order phase transition by using the equilibrium MC method. However, the short-time provides a much easier way to determine the metastability.

Finally, we note that $(d - 2\beta/\nu)/z = 0.83(1)$ which is twice the value of the exponent associated with the power law behavior of $|m|$ is not consistent with that of the ordered start which is equal to 1.12(4). To justify this, we say that the phase transition has become strong enough that the exponents obtained from the two initial configurations are not true critical exponents anymore. In other words, there is different pseudo-scaling behavior associated with each initial configuration which should not be expected to be the same.

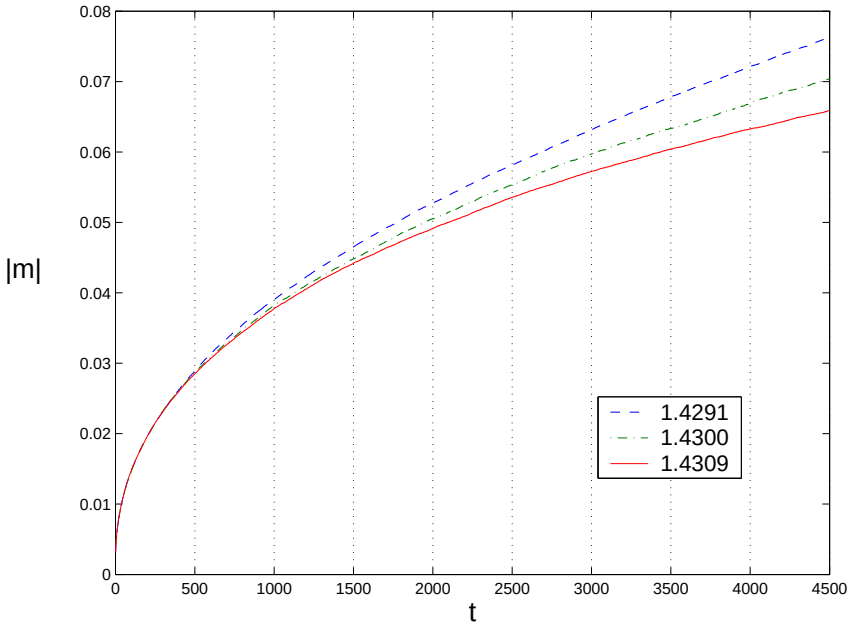

(a)

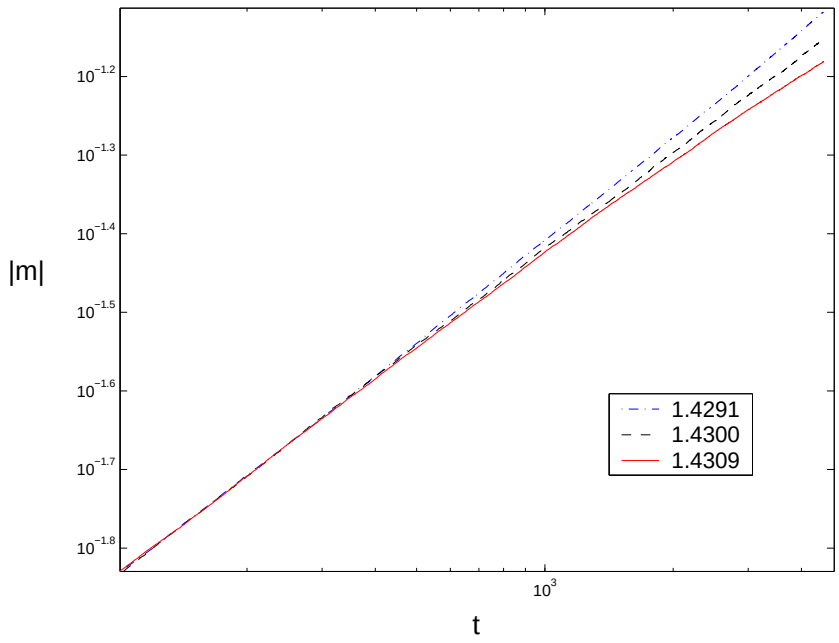

(b)

Figure 6.30: $|m|$ versus t for three temperatures (a) on a linear scale and (b) on a log-log scale

Chapter 7

SUMMARY AND OUTLOOK

7.1 Summary

In frustrated systems, the energy of the interactions between all the particles cannot be minimized simultaneously. Frustration may arise due to either competing interactions or geometry. The nature of the phase transition associated with these systems has been under discussion for more than 25 years. In particular, there is no general agreement on the critical behavior of antiferromagnets on a stacked triangular lattice, the so-called STA model. The GS of such a system for $n = 2$ and $n = 3$ spin components is a 120° structure. The non-collinear nature of the GS leads to the appearance of new degrees of freedom, the so-called chiral degrees of freedom. In addition, it makes the BS associated with these systems different from the common BS of the systems belonging to the Wilson-Fisher universality class. This leads to some peculiar and unpredictable characteristics in critical behavior of these systems.

Frustrated systems, and in particular the STA model, have been investigated by means of the experimental, theoretical and numerical approaches. All these studies have come to a variety of conclusions. The experimental studies have reported a second order phase transition but with the critical exponents that differ from one material to another. This questions the existence of universality and is inconsistent with a second order phase transition. The numerical studies have also found that universality is violated since the STA and STAR models exhibit different critical behavior. On the theoretical side, the situation is controversial because various field theoretical renormalization schemes have led to inconsistent results.

In this thesis, we have introduced a generalized model which is associated with a constraint parameter r. By tuning r, we are able to approach from the STA model ($r = -\infty$ and $r = 0$) to the STAR model $r = \infty$. In addition, we can change the geometry to that of the Kagome lattice ($r = -0.5$). By means of MC simulation, we have studied the short-time dynamics behavior of the model for a broad range of values of r. This approach provides us an accurate technique to determine the order of the phase transition, and also to calculate T_c and the critical exponents of the model as a function of r.

We have worked with three r cases. The first case corresponds to the range $[-\infty, -1]$ where the spins in each plaquette interact ferromagnetically. The $-\infty$ limit corresponds to the STA model. The GS in this case is characterised by a non-collinear 120^0 structure of plaquettes which have the internal spins aligned. We have found that the critical exponents of the model for the r values in this range do not strongly depend on the constraint parameter. This is interesting since it shows that the nature of phase transition is not dependent on the details of the molecular-scale interactions. In other words, by increasing $|r|$, the ferromagnetic interactions within the plaquettes becomes stronger, but the critical behavior does not change. We have discussed this universal behavior in the following way. Because the spins of each plaquette are in parallel alignment, no chirality is defined for each plaquette, and a change in the value of r does not modify the interactions responsible for the non-collinear structure of the system. As a result, the non-collinear nature of the system does not vary. It seems that the critical behavior does not change as long as the non-collinear nature of the system is not modified.

The second case is described by $[0, \infty]$ range of r values. For $r = 0$, we obtained T_c and critical exponents consistent with the previous studies of the STA model. In addition, we found the gradual approach of these values to those of the STAR model as r increases. This has been a success for the model and the method we have used. In contrast to the $[-\infty, -1]$ case, the critical exponents were found to be r

dependent. This means that, by tuning r, the critical behavior changes as the BS remains constant. This non-universal critical behavior is inconsistent with a second order phase transition. Hence we conclude that the phase transition is a weak first order phase transition.

Another indication of a first order phase transition can be the negative value of the anomalous dimension η for all values of r. The critical exponent η becomes more negative as r increases from zero which means that the phase transition becomes stronger first order. This claim has been confirmed by the measurement of metastability. We introduced a parameter called the metastability parameter based on the differences of the transition temperatures associated with the two initial configurations (ordered and disordered configuration). We have found that it generally increases as r becomes larger.

The STA model is found to undergo the weakest first order transition in the $[0, \infty]$ range. We have discussed the reason by introducing the concept of local symmetry. In addition, we expected the STAR model to have the strongest first order phase transition. To investigate it and also regarding the fact that r cannot get very large due to the single-spin flip characteristic of our heat-bath algorithm, we have performed a special simulation for the STAR model using the Metropolis algorithm. We have obtained a T_c and critical exponents consistent with those of the previous study of the STAR model. The anomalous dimension was found to be the most negative compared to those of the finite values of r. The metastability parameter was also found to be the largest which shows that the phase transition is the strongest first order in the $[0, \infty]$ range. As a result, our results strongly suggest that the phase transition associated with this type of system is first order.

The last case of our study was the $(-1, 0)$ case. In this range, the $r = -0.5$ case corresponds to the stacked Kagome antiferromagnet and is a forbidden value since it changes the symmetry of the triangular lattice. It is worth mentioning that on the either side of $r = -0.5$, the GS structure is different. The short-time dynamics scaling

of the ordered configuration runs revealed that the critical exponents β and ν decrease as r approaches $r = -0.5$ from both sides. β was found to fall faster than ν which leads to a decrease in the value of the anomalous dimension. As a result, η becomes even more negative than that of the STAR model. The rate of decrease in β is larger for the r values closer to $r = -0.5$. In particular, for $r = -0.49$, we have found that the relaxation is very slow and also logarithmic. This leads to $\beta = 0$ which implies that the phase transition (if any) is first order. In a similar way, the simulation for $r = -0.505$ has shown that the relaxation is also very slow, which means that β is very small. However, we have not been able to obtain any logarithmic or power law relaxation for $r = -0.505$. This indicates that the nature of the relaxation, and so the phase transition, is different on either side of $r = -0.5$.

7.2 Outlook

We argued that our heat-bath algorithm is a single-spin flip algorithm and not efficient for large values of $|r|$. One can modify it to have a "plaquette flip" algorithm in a sense that it can update a plaquette as a whole and not just one spin. As a consequence, the algorithm will be efficient for large r.

As discussed before, for the STA model, the magnetic and chiral transition take place at the same temperature. The question remains whether the variation of r, specially in the positive r region, separates these two transition temperatures. In fact, this might be a good explanation of why the critical behavior of these systems changes. In our study, we only have measured the magnetic order parameter. However, one can measure the chiral order parameter [53] to investigate if there is a considerable difference between the two transition temperatures for different values of r.

We have not paid as much attention to the $(-1, 0)$ range of r as might be needed. In fact, there is more to do in that range. It was mentioned that we are not aware of any study of the stacked Kagome lattice. One can perform equilibrium MC cal-

culations to investigate its GS structure. One can define different types of order parameters and see how each one behaves as a function of temperature. This will tell us if there is any finite temperature phase transition. From the short-time relaxation point of view, we found that t_{min} increases as r goes to $r = -0.5$. In particular, for $r = -0.505$, we argued that the scaling behavior might emerge after the maximum time at which the simulation is stopped. Therefore one might have to increase t_{max} considerably in order to investigate some of the possibilities.

In our generalized model, we have an infinite range of the r values. This important property has enabled us to interpolate smoothly between different frustrated models. However, for all values of r, the chirality degrees of freedom are present. On the other hand, we know that the peculiar nature of the phase transition associated with these systems is mostly due to the appearance of the chiral degrees of freedom. So one may be interested in interpolating between collinear and non-collinear systems. To do so, we could introduce a Hamiltonian as follows

$$H = -J \sum_{k=1}^{2} \sum_{<ij>} \vec{S}_{ik} \cdot \vec{S}_{jk} \; - \; p \; \sum_{i} (\vec{S}_{i1} \times \vec{S}_{i2})^2 \tag{7.1}$$

where $\vec{S}_{i2}$ and $\vec{S}_{i1}$ are n component classical vector spins which form a spin pair on site i and J is the interaction constant between neighboring spins of the same label. For $p \leq 0$, the system is collinear, however it is non-collinear for $p > 0$. For $p = \infty$, the model corresponds to the dihedral model which has rather consistent critical exponents with the STAR model. The model reduces to a ferromagnetic system with $SO(n)/SO(n-1)$ BS. The study of such a model could tell us how the appearance of chiral degrees of freedom affects the critical behavior.

BIBLIOGRAPHY

[1] L. Onsager. *Phys. Rev.*, **65**:117, 1944.

[2] J. A. Hertz. *Phys. Rev. B*, **14**:1165, 1976.

[3] Hikaru Kawamura. *J. Phys.: Condens. Matter*, **10**:4707, 1998.

[4] J. Binney, N. Dowrick, A. Fisher, and M. Newman. *The Theory of Critical Phenomena*. Oxford Science Publications, 1993.

[5] N. D. Mermin. *Rev. Mod. Phys.*, **51**:591, 1979.

[6] M. E. Fisher et al. *Phys. Rev. Lett*, **28**:1972, 1972.

[7] U. Wolff. *Phys. Rev. Lett.*, **62**:361, 1989.

[8] R. Swendsen and J.Wang. *Phys. Rev. Lett.*, **58**:68, 1987.

[9] N. Metropolis et al. *J. Chem Phys.*, **21**:1087, 1953.

[10] A. Jaster, J. Mainvile, L. Schülke, and B. Zheng. *J. Phys. A*, **32**:1395, 1999.

[11] L. Schülke. *arXiv:hep-lat/0007003v1*, 2000.

[12] P. R. Bevington and D. K. Robinson. *Data reduction and error analysis for the physical sciences*. Boston : McGraw-Hill, 2003.

[13] D. P. Landau and Kurt Binder. *A Guide to Monte Carlo Simulations in Statistical Physics*. Cambridge University Press, 2000.

[14] V. Privman. *Finite size scaling and numerical simulation of statistical systems.* World Scientific, Singapore, 1990.

[15] K. Binder. *Z. Phys. B..*, **43**:119, 1981.

[16] J. M. Kosterlitz and D. J. Thouless. *J. Phys. C*, **6**:1181, 1973.

[17] J. M. Kosterlitz. *J. Phys. C*, **7**:1046, 1974.

[18] H. Kawamura. *J. Phys. Soc. Japan*, **56**:474, 1987.

[19] D. Loison. In H.T. Diep, editor, *Frustrated Spin Systems*, page 181. World Scientific, 2000.

[20] H. B. Weber, T. Werner, J. Wosnitza, H. v. Lohneysen, and U. Schotte. *Phys. Rev. B*, **54**:15924, 1996.

[21] B. D. Gaulin, T. E. Mason, M.F. Collins, and J. F. Larese. *Phys. Rev. Lett.*, **62**:1380, 1989.

[22] T. E. Mason, M. F. Collins, and B. D. Gaulin. *J. Phys. C*, **20**:L945, 1987.

[23] Y. Ajiro, T. Nakashima, Y. Unno, H. Kadowaki, M. Mekata, and N. Achiwa. *J. Phys. Soc. Japan*, **57**:2648, 1988.

[24] T. E. Mason, B. D. Gaulin, and M. F. Collins. *Phys. Rev. B*, **39**:586, 1989.

[25] J. Wang, D. P. Belanger, and B. D. Gaulin. *Phys. Rev. Lett.*, **66**:3195, 1991.

[26] R. Deutshmann, H. van Löhneysen, J. Wosnitza, R. K. Kremer, and D. Visser. *Euro. Phys. Lett.*, **17**:637, 1992.

[27] H. Kadowaki, S. M. Shapiro, T. Inami, and Y. Ajiro. *J. Phys. Soc. Japan*, **57**:2640, 1988.

[28] H. Weber, D. Beckmann, J. Wosnitza, H. von Löhneysen, and D. Visser. *Int. J. Mod. Phys. B*, **9**:1387, 1995.

[29] M. Enderle, G. Fortuna, and M. Steiner. *J. Phys.: Condens. Matter*, **6**:L385, 1994.

[30] M. Enderle, R. Schneider, Y. Matsuoka, and K. Kakurai. *Physica B*, **234-236**:554, 1997.

[31] B. Delamotte, D. Mouhanna, and M. Tissier. *Phys. Rev. B*, 2004.

[32] H. Kadowaki, K. Ubokoshi, K. Hirakawa, J. L. Martinez, and G. Shirane. *J. Phys. Soc. Japan*, **56**:4027, 1987.

[33] J. Wosnitza, R. Deutschmann, H. von Löhneysen, and R. K. Kremer. *J. Phys. Condens. Matter*, **6**:8045, 1994.

[34] Oohara Y, Kadowaki H, and Iio K. *J. Phys. Soc. Japan*, **60**:393, 1991.

[35] K. Koyama and M. Matsuura. *J. Phys. Soc. Japan*, **54**:4085, 1985.

[36] L. P. Kadanoff et al. *Rev. Mod. Phys.*, **39**:395, 1967.

[37] H. Kawamura. *Phys. Rev. B*, **38**:4916, 1988.

[38] H. Kawamura. *Phys. Rev. B*, **42**:2610, 1990.

[39] S. A. Antonenko, A. I. Sokolov, and K. B. Varnashev. *Phys. Lett.*, **208A**:161, 1995.

[40] S. A. Antonenko and A. I. Sokolov. *Phys. Rev. B*, **49**:15901, 1994.

[41] T. Jolicoeur. *Europhys. Lett.*, **30**:555, 1995.

[42] A. Pelissetto, P. Rossi, and E. Vicari. *Phys. Rev. B*, **63**:140414(R), 2001.

[43] P. Calabrese, P. Parruccini, A. Pelissetto, and E. Vicari. *Phys. Rev. B*, **50**:174439, 2004.

[44] P. Calabrese, P. Parruccini, and A. I. Sokolov. *Phys. Rev. B*, **66**:180403R, 2002.

[45] P. Azaria, B. Delamotte, and T. Jolicoeur. *Phys. Rev. Lett.*, **64**:3175, 1990.

[46] Gil Zumbach. *Phys. Rev. Lett..*, **71**:2421, 1993.

[47] M. Tissier, B. Delamotte, and D. Mouhanna. *Phys. Rev. Lett.*, **84**:5208, 2000.

[48] M. Tissier, D. Mouhanna, and B. Delamotte. *Phys. Rev. B*, **61**:15327, 2000.

[49] J. Zinn-Justin. *Quantum Field Theory and Critical Phenomena*. Oxford University Press, New York, 4rd ed., 2002.

[50] A. Dorby and H. T. Diep. *Phys. Rev. B*, **51**:6731, 1995.

[51] D. Loison and K. D. Schotte. *Eur. Phys. J. B*, **14**:125, 2000.

[52] Hikaru Kawamura. *J. Phys. Soc. Japan*, **61**:1299, 1992.

[53] M.L. Plumer and A. Mailhot. *Phys. Rev. B*, **50**:6854, 1994.

[54] T. Bhattacharya, A. Billoire, R. Lacaze, and T. Jolicoeur. *J. Phys. I (Paris)*, **4**:181, 1994.

[55] D. Loison and H. T. Diep. *Phys. Rev. B*, **50**:16453, 1994.

[56] M. Itakura. *J. Phys. Soc. Japan*, **72**:74, 2003.

[57] H. K. Janssen, B. Schaub, and B. Schmittmann. *Z. Phys. B.*, **73**:539, 1989.

[58] B. Zheng. *Phys. Rev. Lett.*, **77**:679, 1996.

[59] B. Zheng. *Physica A*, **283**:80, 2000.

[60] L. Schülke and B. Zheng. *Phys. Rev. E*, **62**:7482, 2000.

[61] S. Bekhechi, B. W. Southern, A. Peles, and D. Mouhanna. *Phys. Rev. E*, **74**:016109, 2006.

[62] A. Peles, B. W. Southern, B. Delamotte, D. Mouhanna, and M. Tissier. *Phys. Rev. B*, **69**:220408(R), 2004.

[63] D. Schmalfuß, J. Richter, and D. Ihle. *Phys. Rev. B*, **70**:184412, 2004.

[64] A. B. Harris, C. Kallin, and A. J. Berlinsky. *Phys. Rev. B*, **45**:2899, 1992.

[65] J. T. Chalker et al. *Phys. Rev. Lett.*, **68**:885, 1992.

[66] D. Huse and A. Rutenberg. *Phys. Rev. B*, **45**:7536, 1992.

[67] J. N. Reimers and A. J. Berlinsky. *Phys. Rev. B*, **48**:9539, 1993.

[68] Heiko Rieger. *Phys. Rev. B*, **52**:6659, 1995.

Appendix A

THE RIGHT DISTRIBUTION OF $COS(\theta)$

We have found the following probability distribution for $\cos(\theta)$

$$P(\theta, \phi) = C \exp(b_{ieff} \cos(\theta)). \tag{A.1}$$

We need a formula which converts the uniform distribution of the random numbers on the interval $[0, 1]$ to the right distribution for $\cos(\theta)$ as given in equation (A.1). The noramlization constant C depends on the value of b_{ieff} and is given by

$$\begin{aligned} 1/C &= \int_0^{2\pi} \int_0^{\pi} \exp\left(b_{ieff} \cos(\theta)\right) \sin(\theta) d\theta d\phi \\ &= 4\pi \sinh\left(b_{ieff}\right)/b_{ieff} \end{aligned} \tag{A.2}$$

As a result, the normalized probability distribution is

$$P(\theta, \phi) = \frac{b_{ieff} \exp(b_{ieff} \cos(\theta))}{4\pi \sinh\left(b_{ieff}\right)}. \tag{A.3}$$

Because the contribution of the intergral over ϕ is just a factor of 2π, we can write the probability distribution just for $\cos(\theta)$ as

$$P(cos(\theta)) = \frac{b_{ieff} \exp(b_{ieff} \cos(\theta))}{2 \sinh\left(b_{ieff}\right)}. \tag{A.4}$$

For a variable y which is distributed according to the probability density $P(y)$, we can define a cumulative probability distribution

$$P_c(Y) = \int_{-\infty}^{Y} P(y) dy \tag{A.5}$$

which gives the probability that $y \leq Y$. By setting $P_c(Y) = r1$ where $r1$ is a uniformly distributed random variable on $[0, 1]$, and then solving the equation for Y, we are able

to create an appropriate probability distribution of Y as a function of $r1$. In our case, we have

$$P_c(cos(\Theta)) = \int_{-1}^{cos(\Theta)} P(cos(\theta))\, dcos(\theta) = r1. \tag{A.6}$$

The integral equation can be reduced to

$$\frac{e^{(b_{ieff}\cos(\Theta)} - e^{-b_{ieff}}}{e^{b_{ieff}} - e^{-b_{ieff}}} = r1. \tag{A.7}$$

which can be easily solved for $\cos(\Theta)$. Hence the final formula is

$$\cos(\Theta) = 1 + \ln[(1 - r1)exp(-2b_{ieff}) + r1]/b_{ieff} \tag{A.8}$$

which provides the right distribution of $\cos(\Theta)$ in terms of the uniform distribution of $r1$ on the unit interval $[0, 1]$.